UNIVERSITY OF CALIFORNIA, SAN DIEGO

Mechanistic Insights into Reactivation of Organophosphate-Conjugated Acetylcholinesterase by Nucleophiles as Antidotes

A Thesis submitted in partial satisfaction of the requirements for the degree Master of Science

in

Biology

by

William Charles Hou

Committee in charge:

Professor Palmer Taylor, Chair
Professor Darwin Berg, Co-Chair
Professor Eva-Maria Collins

2017

The Thesis of William Charles Hou is approved and it is acceptable in quality and form for publication on microfilm and electronically:

Co-Chair

Chair

University of California, San Diego

2017

TABLE OF CONTENTS

LIST OF ABBREVIATIONS

AChE	Acetylcholinesterase
OP	Organophosphate
OP-AChE	Organophosphate-conjugated acetylcholinesterase
ATCh	Acetylthiocholine
EMP-MeCyC	ethyl([3-cyano-4-methyl-7-hydroxy]coumarinyl)methylphosphinate
POX	Paraoxon
2-PAM	Pralidoxime
D-2-PAM	Deuterated pralidoxime
D-RS194B	Deuterated RS194B
D_2O	Deuterium oxide
DTNB	(5,5'-dithiobis-(2-nitrobenzoic acid))
Ser (S)	Serine
His (H)	Histidine
Glu (E)	Glutamate
Trp (W)	Tryptophan
Tyr (Y)	Tyrosine
Gly (G)	Glycine
Ala (A)	Alanine

LIST OF FIGURES

LIST OF TABLES

ACKNOWLEDGEMENTS

I would like to thank Dr. Palmer Taylor as a thesis advisor, committee chair, and mentor for both my projects and as a researcher. I am very grateful for the chance to work with someone who holds so much respect for science and others.

I would also like to thank Dr. Darwin Berg and Dr. Eva-Maria Collins for being members of my committee.

I would like to thank Dr. Zoran Radic for his feedback and assistance on my research.

Finally, I would like to thank all the members of the Taylor lab, including Limin Zhang, Joannie Ho, and Andrea Camacho, who have assisted me since the first day I started working in the Taylor lab.

The Materials and Methods section, in part is currently being prepared for submission for publication of the material with coauthors Zoran Radic, Palmer Taylor, and Limin Zhang. The thesis author was the primary author of this material.

The Results section, in part is currently being prepared for submission for publication of the material with coauthors Zoran Radic, Palmer Taylor, and Limin Zhang. The thesis author was the primary author of this material.

ABSTRACT OF THE THESIS

Mechanistic Insights into Reactivation of Organophosphate-conjugated Acetylcholinesterase by Nucleophiles as Antidotes

by

William Charles Hou

Master of Science in Biology

University of California, San Diego, 2017

Professor Palmer Taylor, Chair
Professor Darwin Berg, Co-Chair

Organophosphates (OP) interacting with acetylcholinesterase (AChE) carry limited therapeutic benefits and are effective biodegradable insecticides when used judiciously. However, certain volatile OP's have been used insidiously in terrorism. Current drugs that reactivate AChE and are used to combat the inhibitory effects of OP's

are oximes, but the mechanism by which these oximes act in the gorge of the enzyme is not well-understood. General base catalysis dictates that the oximate anion acts as a nucleophile against the organophosphate esters, which is consistent with in-solution pH dependent oximolysis reactions. I employed pH dependent oxime-induced reactivations of OP-AChE and looked at kinetic isotope effects for reactivation in order to deconstruct the mechanism in which these oximes nucleophilic attack within the enzyme. My studies found that oxime-induced reactivation optimizes at pH ~7.5, contradictory to general base catalysis. Solvent isotope effects exhibited a reduction in reactivation rates, with different magnitudes of depression for different oximes and respective oxime concentrations. Therefore, the existence of a hydrogen bonding network that contributed to the formation of the oximate anion is proposed. In addition, I studied fluoride-induced reactivation of OP-AChE, which is predicted to operate differently than oximes. These findings showed that fluoride-induced reactivation was enhanced by low pH and higher ionic strength environments.

I.

Introduction

Acetylcholine is an important neurotransmitter responsible for signaling in both the central and peripheral nervous systems. Depolarization of specific presynaptic neurons lead to the exocytosis of this neurotransmitter into the synaptic cleft of cholinergic systems, where it binds to cholinergic receptors located on the postsynaptic neuron or skeletal muscle, thus transducing the neuronal signal downstream to the next cell. Acetylcholinesterase is an enzyme that is responsible for regulating the duration of transmitter action and excess buildup of acetylcholine in the synaptic cleft by catalyzing the hydrolysis of the neurotransmitter.

A. Acetylcholinesterase

Acetylcholinesterase (AChE) is an α/β serine hydrolase that is responsible for catalyzing the hydrolysis of the neurotransmitter acetylcholine (Figure I.1). The active site of AChE is located approximately 20Å from the surface in an aromatically lined gorge, and an asymmetric charge distribution in AChE creates a dipole moment that is parallel to the axis of the gorge (Dvir et al., 2010). The direction of this dipole moment is thought to guide positively charged molecules, such as acetylcholine, into the gorge.

Within the gorge of human AChE is an aromatic anionic site consisting of Trp86, which can bind to the cationic trimethylammonium head group of acetylcholine via cation-Π-electron interactions (Ordentlich et al., 1993). The acyl group of acetylcholine is wedged between the sidechains of Phe295 and Phe297, which constitute the acyl binding

pocket (Ordentlich et al., 1993). The acyl binding pocket contributes to substrate specificity of the enzyme, as larger substrates like butyrylcholine are hydrolyzed at a much slower rate compared to acetylcholine (Ordentlich et al., 1993).

The active site of human AChE contains the catalytic triad consisting of Ser203, His447, and Glu334, which are the main players for acetylcholine hydrolysis (Figure I.2) (Shafferman, et al., 1992). Like many serine hydrolases, the catalytic triad participates in a charge relay system, in which His447 and Glu334 are structured via a hydrogen bonding network and deprotonate Ser203. The deprotonated serine readily nucleophilic attacks the carbonyl carbon of acetylcholine, forming a tetrahedral oxyanion intermediate that is stabilized by the amide hydrogens of the peptide backbone of Gly121, Gly122, and Ala204, which constitute the oxyanion hole (Ordentlich et al., 1998). The tetrahedral intermediate collapses, releasing a choline group and forming an acyl-conjugated serine. Removal of the conjugated acyl group from the serine is very similar to its formation. A water molecule enters the gorge and is deprotonated by His447 and Glu334 via a similar charge relay system. The deprotonated water molecule readily acts to attack the carbonyl carbon of the acyl-enzyme conjugate, forming another tetrahedral intermediate that is stabilized by the oxyanion hole. This tetrahedral intermediate collapses, releasing an acetate molecule from Ser203 and resetting catalytic function in the enzyme.

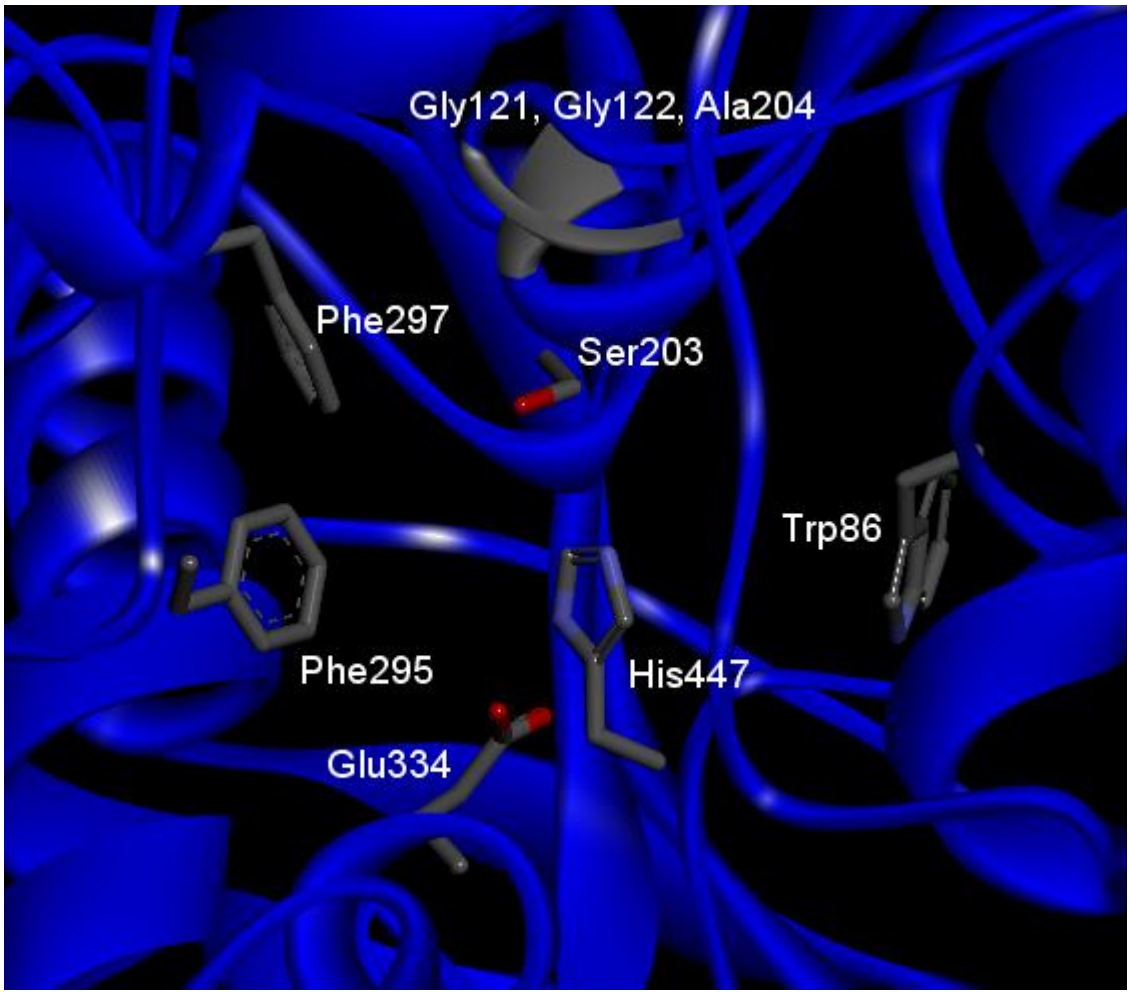

Figure I.1: Crystal structure of the active gorge of acetylcholinesterase (Goldenzweig et al., 2016)

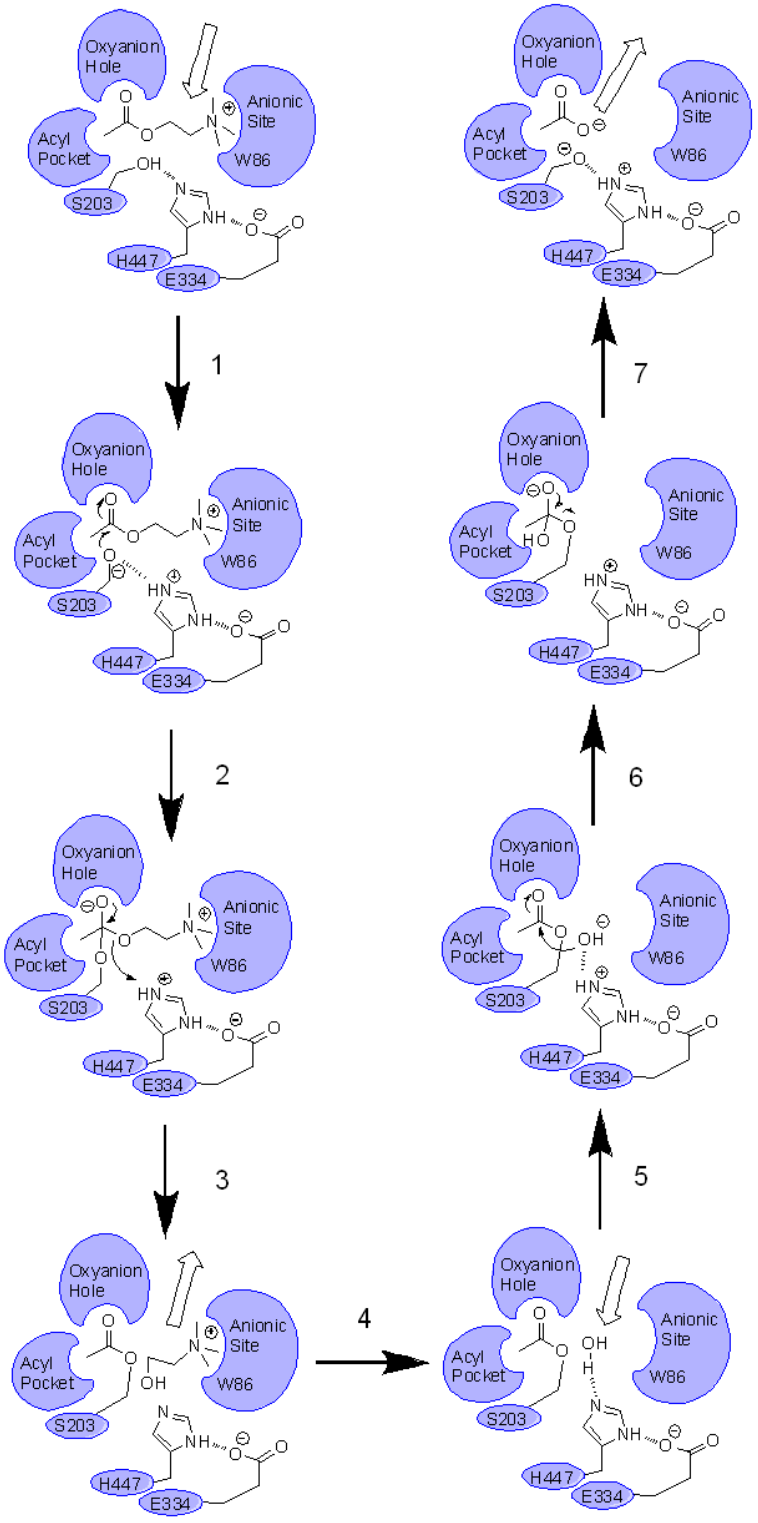

Figure I.2: Catalytic mechanism for the hydrolysis of acetylcholine via acetylcholinesterase

B. Organophosphates

Organophosphates (OP) are organic compounds that are thionoester or oxyester derivatives of phosphate (Figure I.3). They are classed as anticholinesterases for their ability to irreversibly inhibit the catalytic activity of acetylcholinesterase by covalently bonding to Ser203 (Patocka et al., 2005). As a result of their inhibitory effects, OP can be effective biodegradable pesticides when used judiciously, as well as have limited therapeutic applications (Pope et al., 2005). However, they can also be used insidiously as nerve agents, as demonstrated by their use during the assassination of Kim Jong-Nam in February 2017 and the sarin gas attack in Syria in April 2017 (Paddock and Sang-Hun, 2017; Kinsley and Barnard, 2017).

In the nervous system, inhibition of AChE via OP's results in the accumulation of unhydrolyzed acetylcholine. The excess acetylcholine will continuously activate cholinergic receptors on the post-synaptic neuron or muscle endplate and prevent repolarization. Future neuronal signaling in the synaptic network is then halted, which will lead to adverse consequences if left untreated.

The mechanism by which organophosphates inhibit AChE (Figure I.4) is very similar to the addition-elimination reaction of acetylcholine catalysis (Sirin and Zhang, 2014). His447 and Glu334 facilitate the deprotonation of Ser203, allowing for nucleophilic attack on the phosphonyl phosphorus of the organophosphate. The resulting structure is a pentavalent intermediate, which is stabilized by the oxyanion hole similar to the tetrahedral intermediate in acetylcholine catalysis. This intermediate collapses, releasing a leaving group from the OP and forming a phosphonyl or phosphoryl-enzyme conjugate. Phosphonylation is slower than acylation, presumably due to the steric

constraints of the pentavalent intermediate within the gorge, which creates a large energy difference between the pentavalent intermediate and the tetrahedral ground state. Consequently, these steric constraints also contribute to irreversible inhibition, as water is not a sufficiently nucleophilic to react with the tetrahedral phosphonyl-enzyme in order to dephosphonylate the enzyme (Kovarik et al., 2003). Therefore, a stronger nucleophilic alternative is required in order to release the organophosphate from the enzyme.

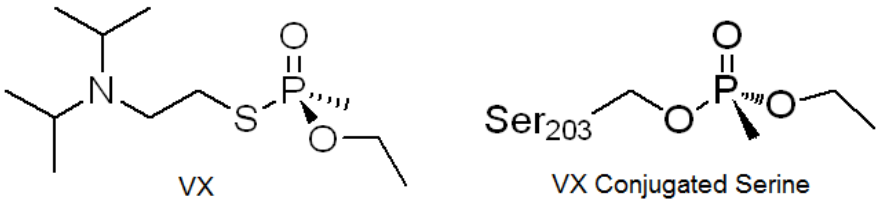

Figure I.3: Chemical structure of the organophosphate VX and its conjugated species after inhibition

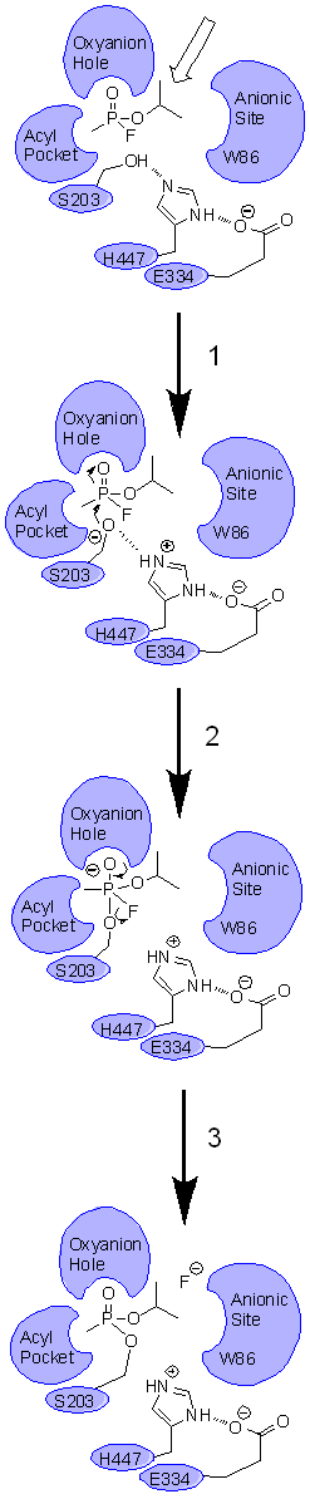

Figure I.4: Mechanism of organophosphate inhibition in acetylcholinesterase

C. Oximes

Strong nucleophilic oximes have demonstrated the ability to free the inhibited acetylcholinesterase from the organophosphate, thus "reactivating" the enzyme via Michaelis-like kinetics (Figure I.5, Table I.1) (Radic et al., 2013). Cationic and zwitterionic oximes, such as pralidoxime and RS194B respectively (Figure 1.6), mimic the cationic nature of acetylcholine, which allows them to follow AChE's dipole moment into the gorge. Within the active site, these oximes can exert a nucleophilic attack on the phophonyl-conjugated serine, releasing a phosphonyl-oxime from the enzyme similar to the deacylation that occurs during acetylcholine hydrolysis (Chunyuan et al., 1999).

Pralidoxime (2-PAM) is a quaternary cationic oxime developed in the 1950s that has been used to treat organophosphate poisoning (Wilson and Ginsburg, 1959). Its efficacy as a reactivator in post-treatment of OP exposure has been widely disputed, but one notable limitation of 2-PAM is its inability to enter the central nervous system (Eddleston et al., 2002). The cationic nature that gifted 2-PAM the ability to readily enter the active gorge of AChE also restricts its permeability across the blood-brain barrier, thus limiting its application.

One answer towards the limitations set by 2-PAM was the development of novel zwitterionic oximes, such as RS194B (Radic et al., 2012). RS194B can form a cationic species that allows the oxime to readily enter the active gorge of AChE, but unlike 2-PAM, RS194B can also form a neutral species, which allows it to cross the blood-brain barrier and function in both the peripheral and central nervous system. Furthermore, the neutral species of RS194B allows for oral bioavailability, which bypasses the need for

sterile environments normally required for parenteral administration and expands its applicability in septic field situations.

While oximes have been shown to reactivate AChE through nucleophilic attack on the phosphonyl-enzyme, the exact mechanism by which these oximes induce reactivation is not well understood. In order for nucleophilic attack to readily occur, the oxime must first be deprotonated into an oximate anion species. If we assume that oxime reactivation follows general base catalysis, that is higher pH conditions would shift the oximate/oxime equilibrium towards its anionic form, then oximes with higher pK_a values would more readily reactivate OP-AChE. The other option is that there are a number of charged amino acid side chains located within the gorge of the enzyme, which could facilitate deprotonation of the oxime. In order to distinguish between these different mechanisms, I performed pH-dependent oxime-induced reactivations of OP-AChE and compared them to oxime-induced nucleophilic attacks in-solution. In addition, I performed kinetic-isotope studies on oxime-induced reactivation of OP-AChE to investigate the existence of a hydrogen bonding network within the enzyme that may facilitate the formation of the oximate anion.

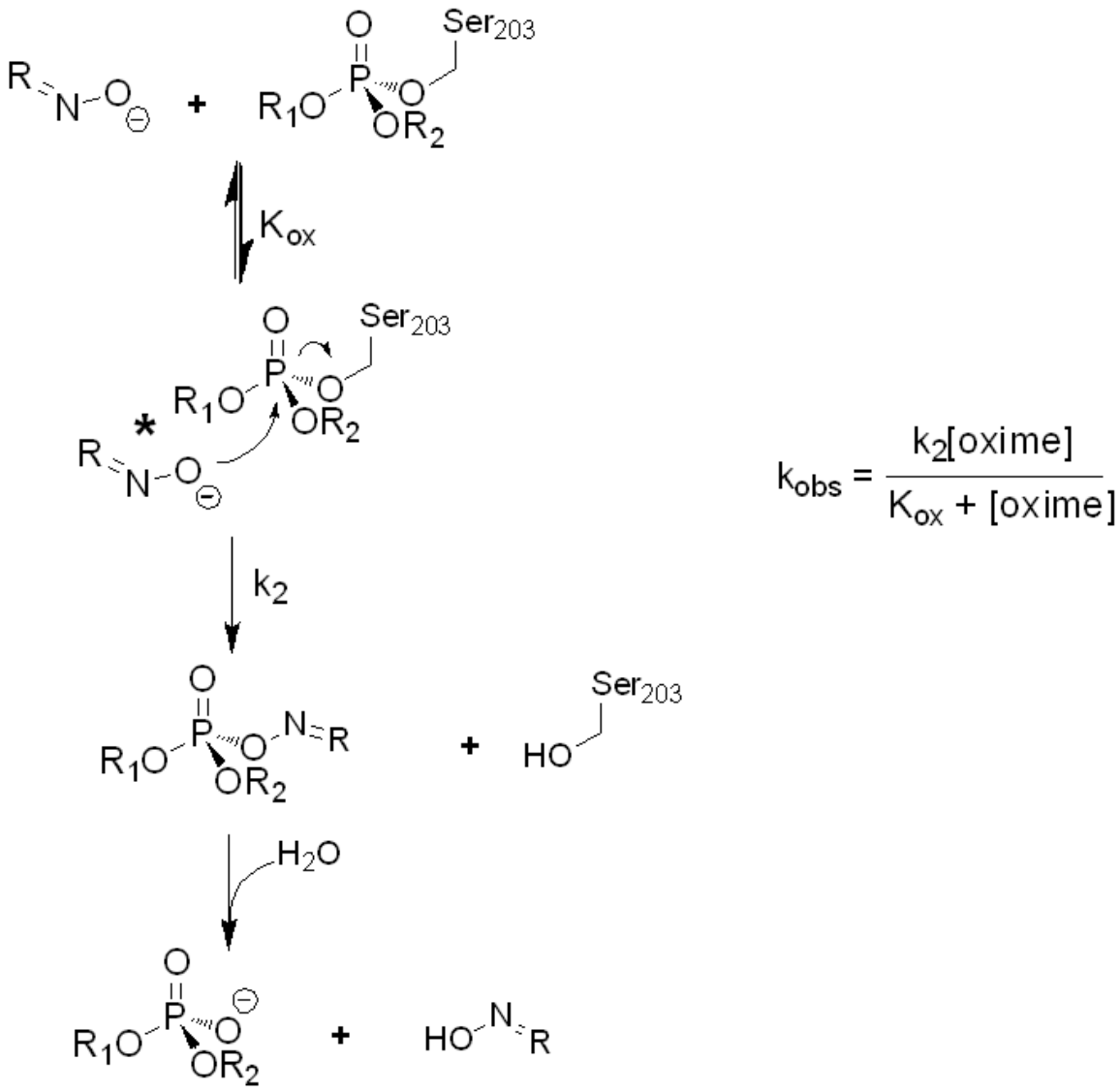

Figure I.5: Mechanism for oxime-induced reactivation of AChE via Michaelis-like kinetics

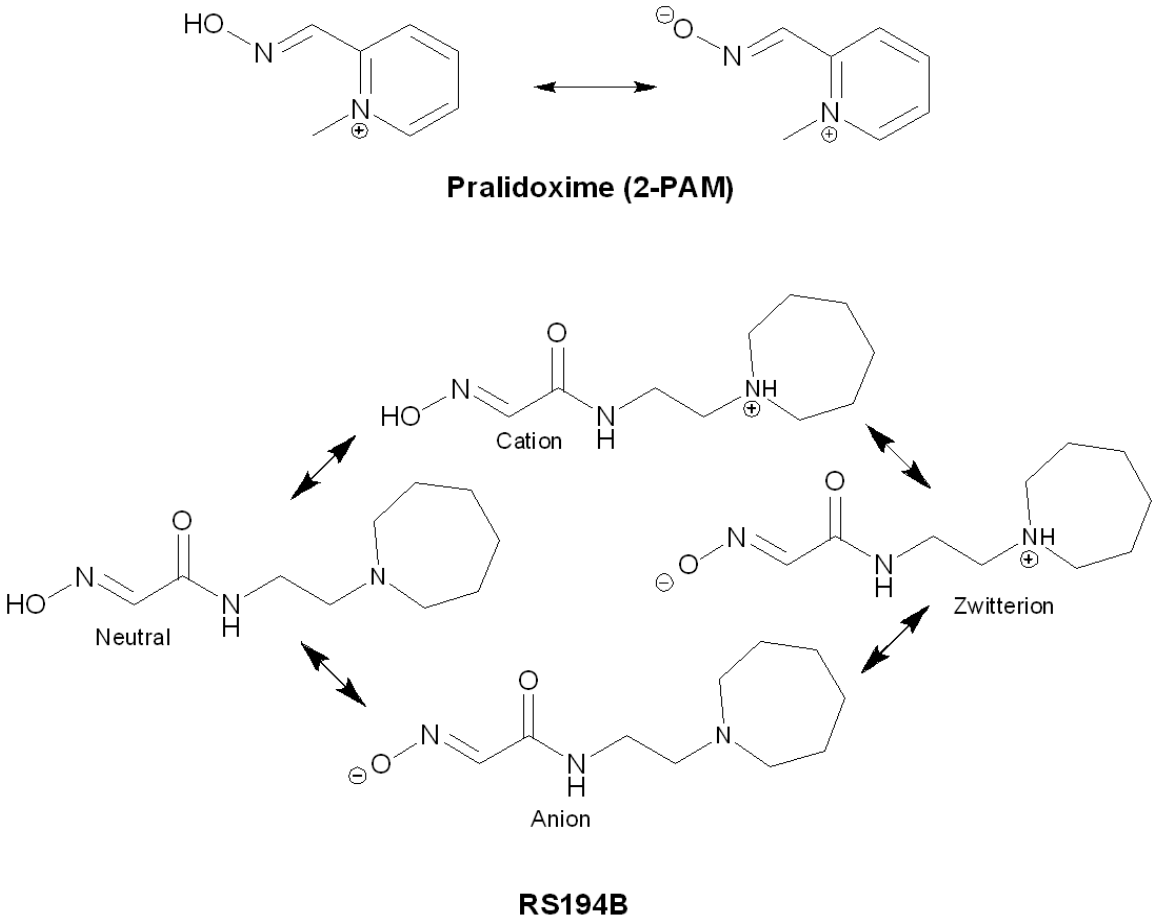

Figure I.6: Chemical structure of pralidoxime (top) and RS194B (bottom). The ionization equilibrium in RS194B allows for cycling among neutral species and various charged species

Table I.1: Summary of pK_a and kinetic constants for RS194B and pralidoxime. Maximal reactivation rate constant is defined by k_2, apparent dissociation constant of oxime*OP-AChE reversible complex is defined by K_{OX}, and overall second order reactivation rate constant is defined by k_r (Radic et al., 2012).

Oxime	pK_a	k_2 (min^{-1})	K_{OX} (mM^{-1})	k_r ($M^{-1}min^{-1}$)
RS194B	8.8	2.8	1.6	1800
Pralidoxime	8.1	0.73	0.3	2400

D. Fluoride Reactivation

One of the earliest studies on fluoride-induced reactivation of organophosphate-conjugated acetylcholinesterase was performed by Swedish scientist Edith Heilbronn (Heilbronn, 1965). Apart from Heilbronn and a few others, the subject of fluoride-induced reactivation is not well-studied, most likely because the pharmacological application of using fluoride to treat organophosphate poisoning is discouraged by the toxic concentrations required to do so.

Previous studies on fluoride-induced reactivation of sarin-inhibited AChE have demonstrated the reconstitution of the sarin organophosphate from the inhibited enzyme, demonstrating that fluoride-induced reactivation operates by direct nucleophilic attack on the phosphonyl-enzyme, similar to oxime-induced reactivation (Polhuijs et al., 1997). However, this sort of mechanism appears to be paradoxical, as the dipole moment of the gorge is thought to draw in cationic molecules, yet the fluoride anion is somehow able to enter the active site and attack the organophosphate. Furthermore, while fluoride is known to be a powerful nucleophile, its nucleophilicity is greatly reduced in polar-protic solvents, such as the aqueous environment in which AChE resides in, imposing yet another difficulty that must be overcome for fluoride-induced reactivation. Finally, fluoride anions have been shown to reversibly inhibit AChE activity via a binding site located in the gorge, although the exact mechanism of this inhibition is not well-understood (Krupka, R., 1966).

While fluoride-induced reactivation may not have any direct pharmacological application, its unique reactivating capabilities is interesting from a mechanistic standpoint. A deeper understanding of this curious mechanism may prove insightful on

the structural dynamics of AChE, which could contribute to oxime or other reactivator designs.

II.

Materials and Methods

A. Materials

Acetylthiocholine iodide, Ellman's reagent (5,5'-dithiobis-(2-nitrobenzoic acid) or DTNB), paraoxon (POX), pralidoxime (2-PAM), lithium chloride, cesium chloride, and lithium fluoride, were purchased from Sigma-Aldrich. Deuterium oxide was purchased from Acros Organics. Cesium fluoride was purchased from Oakwood Chemical. Sodium fluoride and sodium pyrophosphate were purchased from Analytical Reagent. Sodium phosphate monobasic monohydrate, sodium phosphate dibasic anhydrous, sodium phosphate tribasic, sodium chloride, and bovine serum albumin (BSA) were purchased from Fisher Scientific. P-6 polyacrylamide spin columns were purchased from Bio-Rad. The non-volatile VX analogue ethyl([3-cyano-4-methyl-7-hydroxy]coumarinyl)methylphosphinate (EMP-MeCyC) (Figure II.1) was a gift from Dr. Gabriel Amitai of the Israel Institute for Biological Research. The RS194B oxime was a gift from Drs. Rakesh Sit and Barry Sharpless of the Scripps Research Institute at La Jolla.

Purified monomeric wildtype human acetylcholinesterase was prepared according to Sit et al. (Sit et al., 2011).

All spectroscopic experiments were performed using either a Beckman DU640 Spectrophotometer or CARY 1E UV-Visible Spectrophotometer, unless otherwise stated. Buffer solutions made from deuterium oxide had pH/pD correction by adding 0.4 to the pH value read on the pH meter.

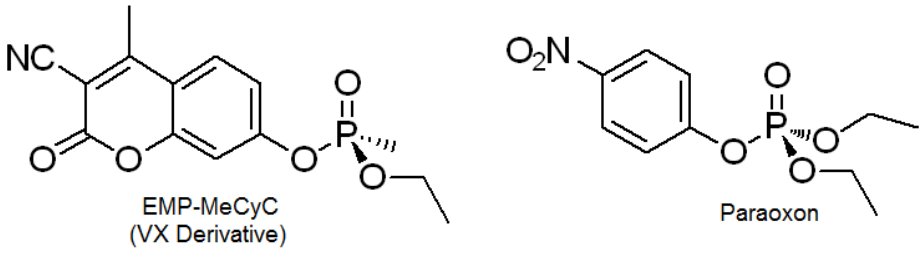

Figure II.1: Chemical structure for VX derivative, ethyl([3-cyano-4-methyl-7-hydroxy]coumarinyl)methylphosphinate, and paraoxon

B. NMR of Deuterated Oximes

Pralidoxime and RS194B were dissolved in 0.1 M sodium phosphate buffer at pD 6.4 that was prepared in deuterium oxide. ^{1}H (600 MHz) NMR spectra of the compounds were recorded at 298 K on a Bruker B-ACS60 spectrometer.

C. Oximolysis of Fluorogenic Organophosphate

Oximolysis of fluorogenic organophosphate (Figure II.2) was performed by reacting 2.5 mM oximes with 0.25 mM EMP-MeCyC VX derivative in 0.1 M sodium, phosphate buffer at varying pH. Reactions conducted at pH > 8.5 were performed in 0.1 M sodium phosphate-pyrophosphate buffer. Aliquots taken over a time course were measured for increasing absorption at 400 nm using a NanoDrop 2000c Spectrophotometer. Pseudo first-order rate constants (k_{obs}) for oximolysis were determined by plotting absorption against the reaction time course and using a logarithmic regression.

D. Oximolysis of Acetylthiocholine

Oximolysis of acetylthiocholine (Figure II.3) was performed by reacting 10 mM oximes with 1 mM acetylthiocholine with 0.3 mM DTNB in 0.1 M sodium phosphate buffer at varying pH. Reactions conducted at pH > 8.5 were performed in 0.1 M sodium phosphate-pyrophosphate buffer. Deuterated reactions were performed with 0.1 M sodium phosphate or sodium phosphate-pyrophosphate buffers that were prepared in deuterium oxide. Pseudo-first order reaction rate constants (k_{obs}) were obtained spectroscopically by measuring the increasing rate of absorbance at 412 nm.

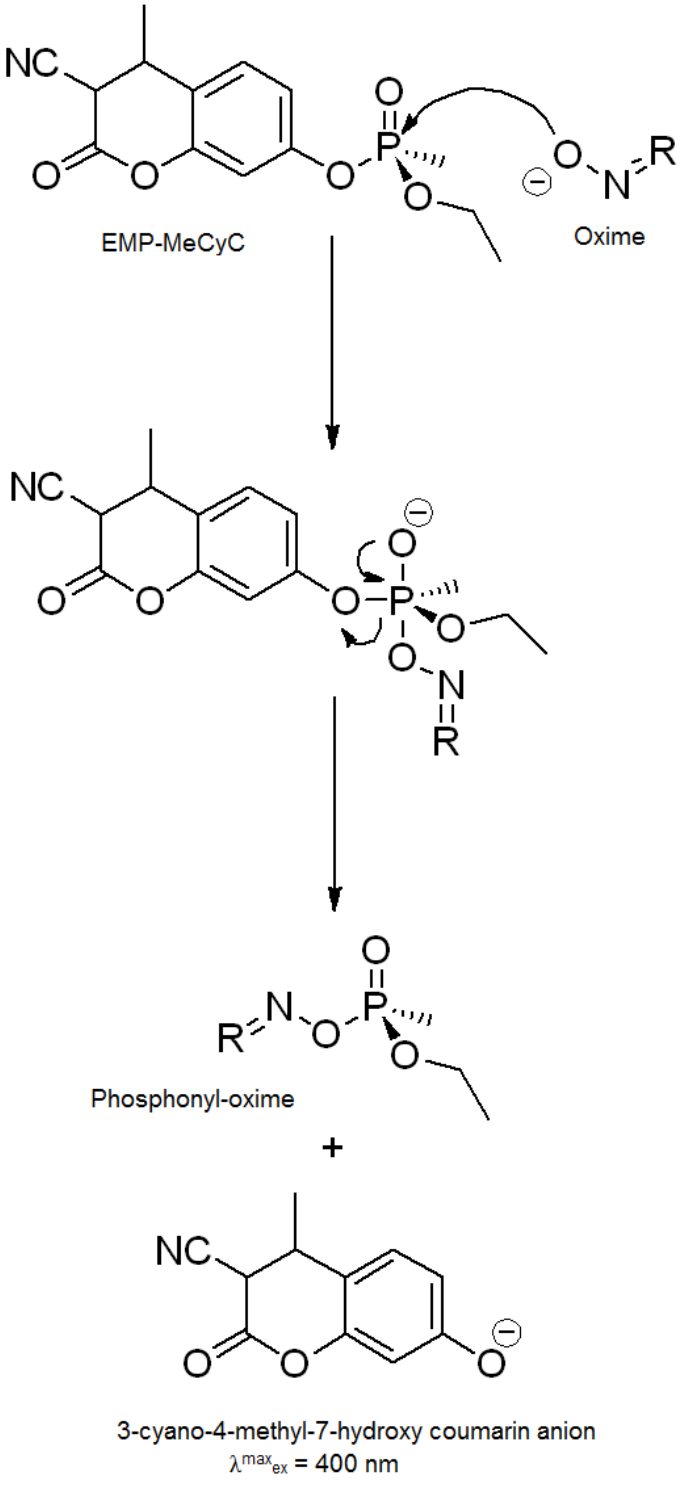

Figure II.2: Reaction mechanism for oximolysis of EMP-MeCyC (Amitai et al., 2007)

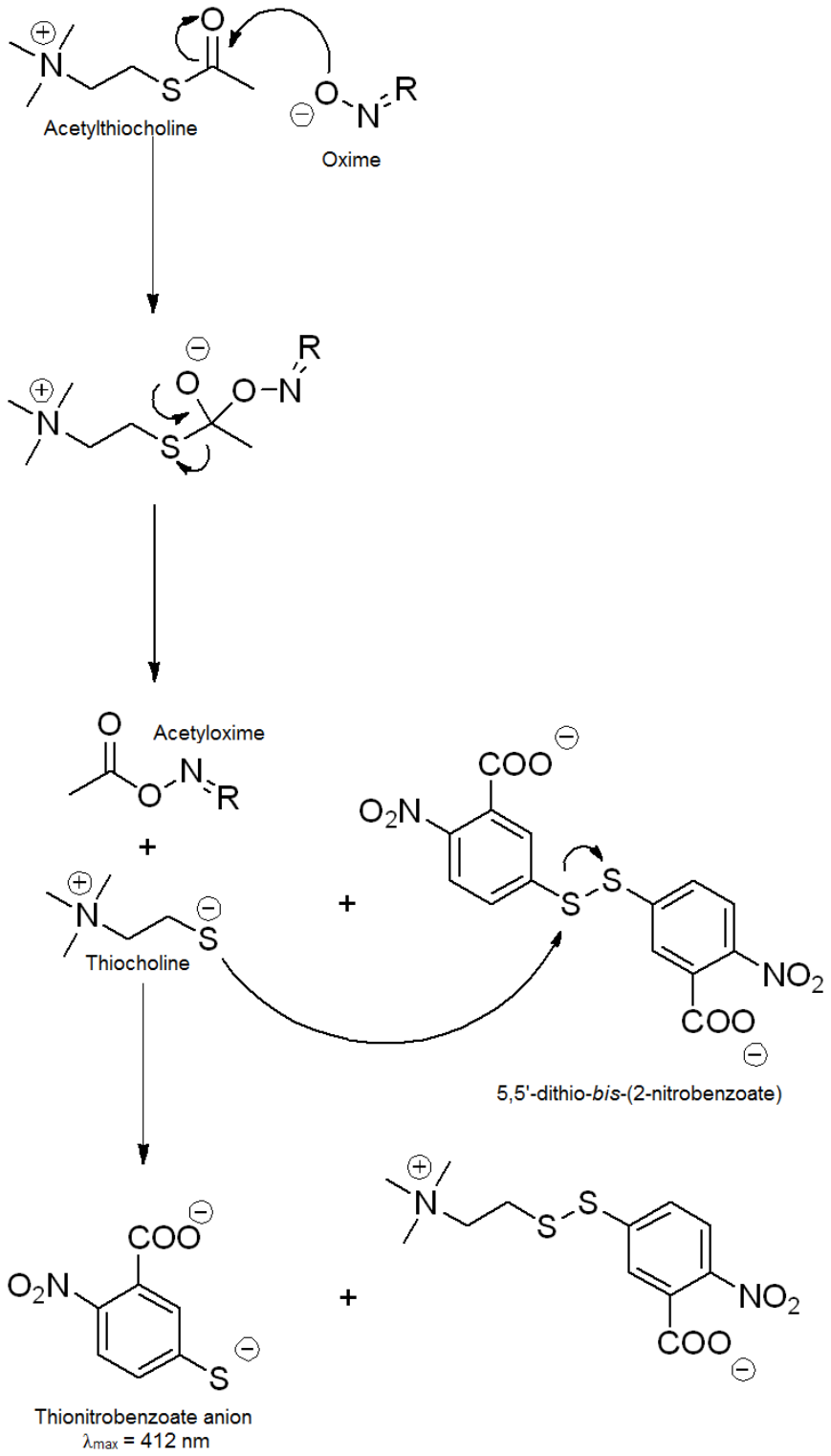

Figure II.3: Reaction mechanism for oximolysis of acetylthiocholine (Ellman et al., 1961)

E. Enzyme Inhibition

Micromolar concentrations of wildtype human AChE with 0.01% BSA in 0.1 M sodium phosphate buffer, pH 7.4, were reacted with four-fold excess organophosphate inhibitor and incubated at 25 ℃ for at least 4 minutes to form the OP-conjugated enzyme. Inhibited enzymes were then subsequently passed through two successive P-6 polyacrylamide spin columns at 2000 RPM for 2 minutes each to separate conjugated AChE from excess OP.

F. Enzyme Reactivation

Picomolar concentrations of organophosphate-inhibited wildtype human AChE in 0.1 M sodium phosphate buffer at varying pH values with 0.01% BSA were incubated at 37 ℃ with reactivating agents at varying concentrations. Reactivation assays at pH > 8.5 were incubated with a 0.1 M sodium phosphate-pyrophosphate buffer with 0.01% BSA. Deuterated reactivations were incubated in 0.1 M sodium phosphate or sodium phosphate-pyrophosphate buffers that were prepared in deuterium oxide with 0.01% BSA. Ionic-strength dependent reactivations had hAChE-WT incubated at 37 ℃ with fluoride salts in 10 mM sodium phosphate buffer at pH 6.5 with 0.01% BSA and varying concentrations of chloride salts that contain the same cation counterion as the fluoride salts.

Reactivation of OP-AChE was monitored by measuring cholinesterase activity by removal of aliquots at varying times during the course of the reactivation. Cholinesterase activity was measured via Ellman assay (Figure II.4) (Ellman et al., 1961). Pseudo first-

order rate constants (k_{obs}) for enzyme reactivation were determined by plotting enzyme activity against the reactivation time course and using a logarithmic regression.

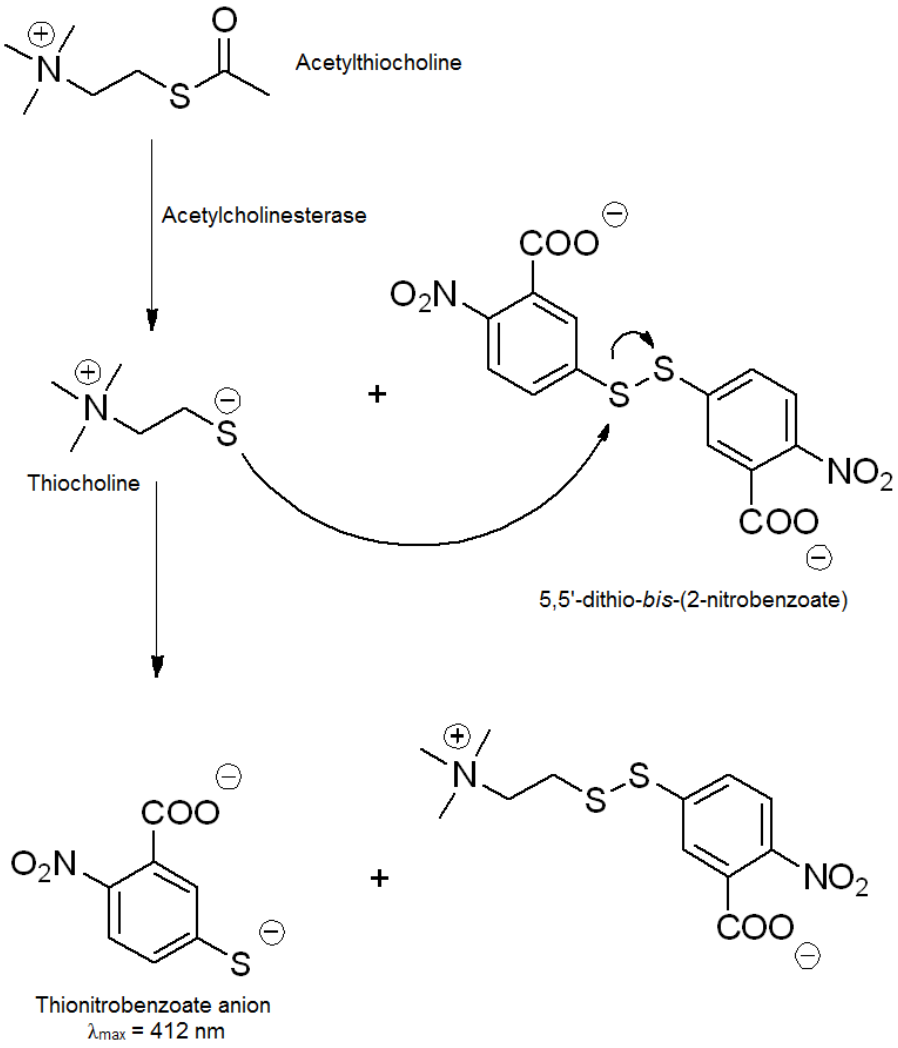

Figure II.4: Reaction mechanism of the Ellman assay used to determine cholinesterase activity (Ellman et al., 1961)

G. Acknowledgement

This section, in part is currently being prepared for submission for publication of the material with coauthors Zoran Radic, Palmer Taylor, and Limin Zhang. The thesis author was the primary author of this material.

III.

Results

A. pH Dependence of Oximolysis

Oximolysis reactions were performed by reacting the oximes 2-PAM or RS194B against EMP-MeCyC fluorogenic VX derivative in buffers ranging from pH 6-11 in order to measure the relative nucleophilicity of the oximes in this pH range. The pseudo-first order rate constants for 2-PAM and RS194B induced oximolysis of EMP-MeCyC at various pH values are summarized in Figure III.1. Oximolysis induced by 2-PAM and RS194B both followed a sigmoidal curve, with rate constants increasing with pH. The points of inflection occurred between pH 8-8.4 for 2-PAM and pH 8.8-9 for RS194B, which is consistent with independent measurements of the pK_a (Radic et al., 2012).

B. pH Dependence of Oxime-Induced Reactivation of Organophosphate-Conjugated Acetylcholinesterase

VX-conjugated hAChE-WT was incubated at 37 ℃ with 2-PAM and RS194B in buffer solutions ranging from pH 6-9.5, and the pseudo-first order rate constants for oxime-induced reactivation of OP-AChE in this pH range are summarized in Figure III.2. Reactivation rates for 2-PAM and RS194B were obtained for oxime concentrations above and below their respective K_{OX} (Radic et al., 2012). 2-PAM and RS194B reactivation rates demonstrated a bell-shaped pH dependence for both oxime concentrations, with peak reactivation rates occurring between pH 7.5-8.

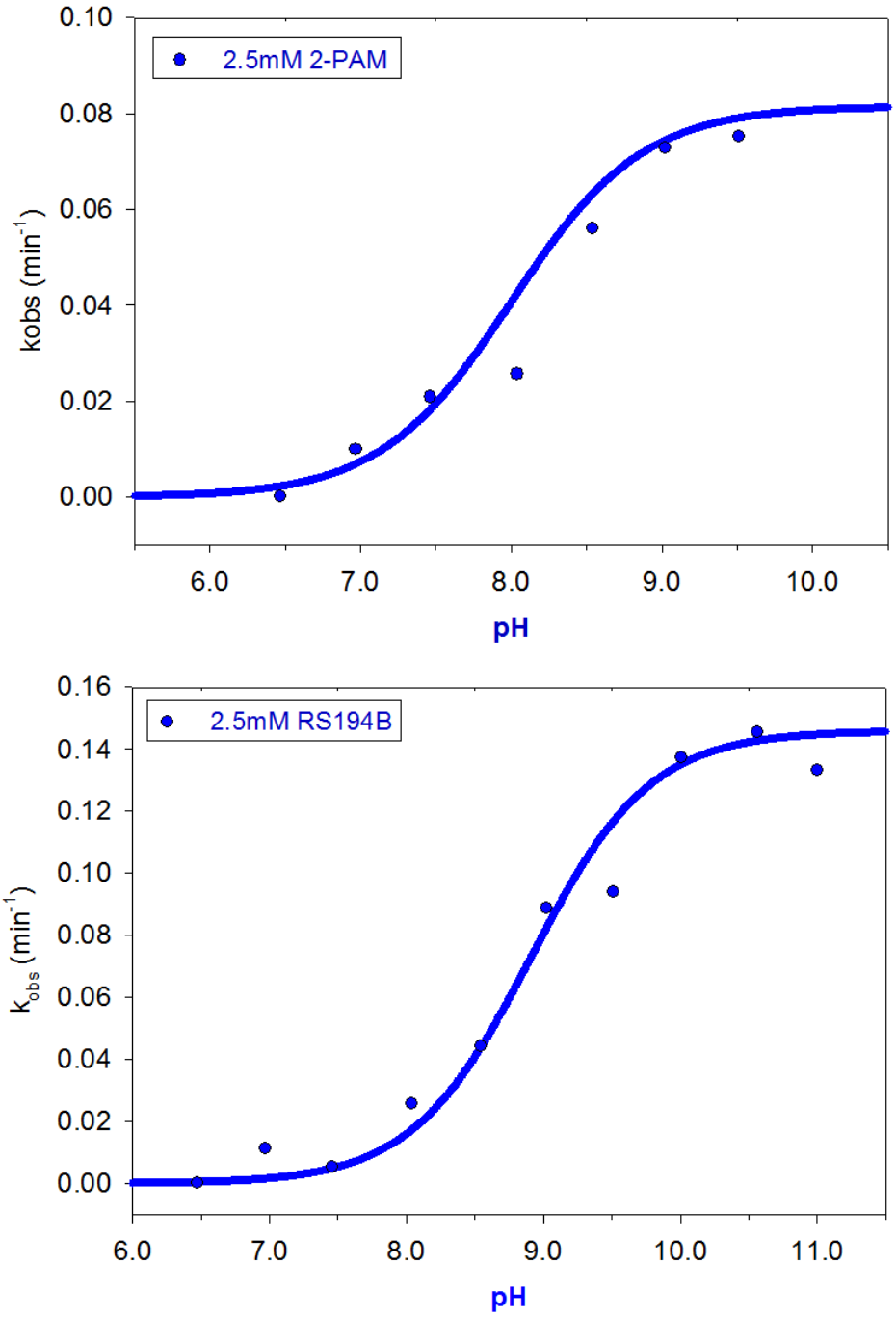

Figure III.1: pH dependencies of pralidoxime (2-PAM) and RS194B oximolysis against EMP-MeCyC. The upper graph shows pH dependence of 2-PAM induced oximolysis while the lower graph shows pH dependence of RS194B induced oximolysis. The pH dependence for 2-PAM and RS194B show points of inflection between pH 8-8.4 and pH 8.8-9 respectively

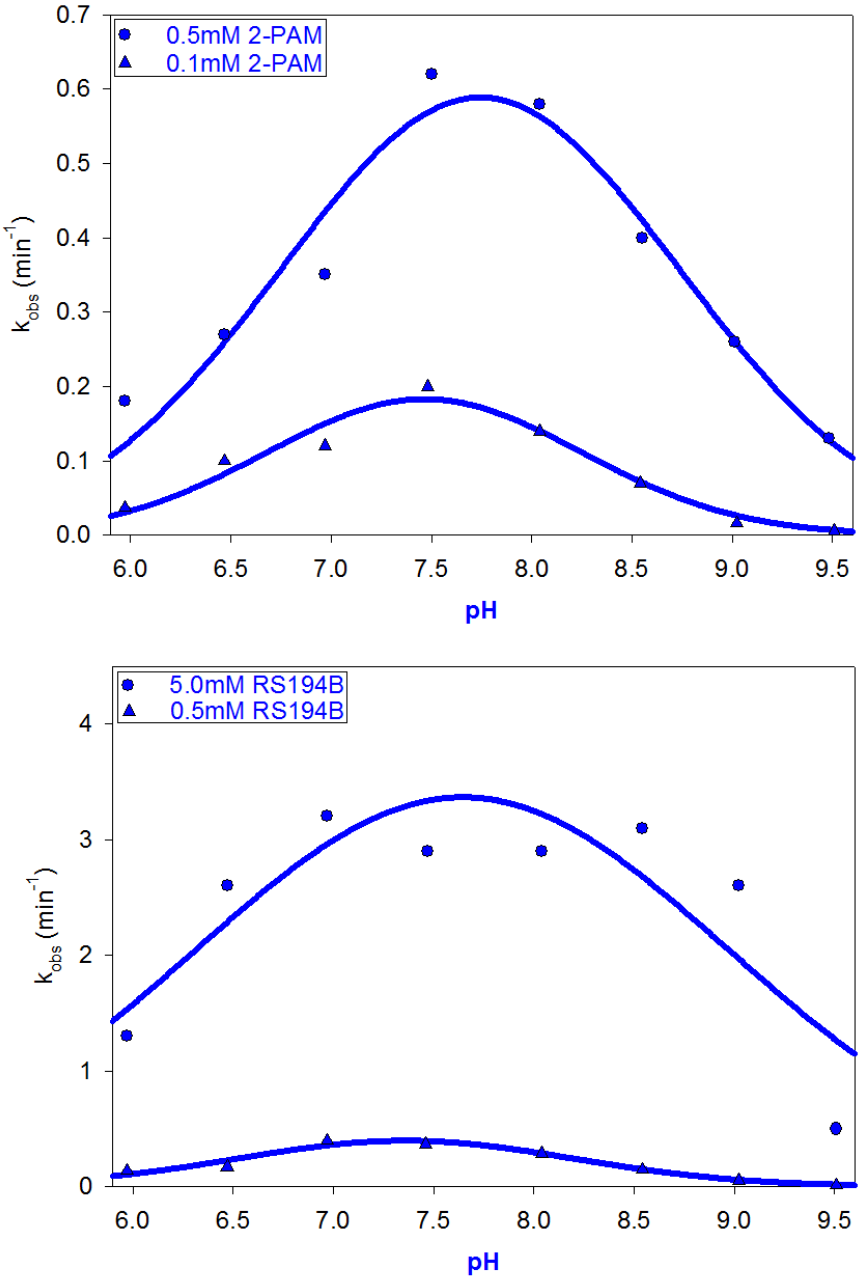

Figure III.2: pH dependencies of pralidoxime and RS194B induced reactivation of VX-conjugated wildtype human acetylcholinesterase. The upper graph shows pH dependence of 2-PAM-induced reactivation rate constants at concentrations above and below its K_{OX}. The lower graph shows pH dependence of RS194B-induced reactivation rate constants at concentrations above and below its K_{OX}. Both oximes exhibited bell-shaped curves, with peak reactivation rates occurring between pH 7.5-8.

C. The Exchangeable Hydrogens for Oximes

2-PAM and RS194B were dissolved in deuterium oxide buffer to allow for rapid hydrogen-deuterium exchange on the oximes. ^{1}H NMR (600 MHz) spectrum and data for 2-PAM (Figure III.3, Table III.1) demonstrate full hydrogen-deuterium exchange of the oxime hydrogen. ^{1}H NMR (600 MHz) spectrum and data for RS194B (Figure III.4, Table III.2) demonstrate full hydrogen-deuterium exchange of the oxime, secondary amide, and azepane amine hydrogens, as well as partial hydrogen-deuterium exchange of the hydrogen located on the aldoxime carbon.

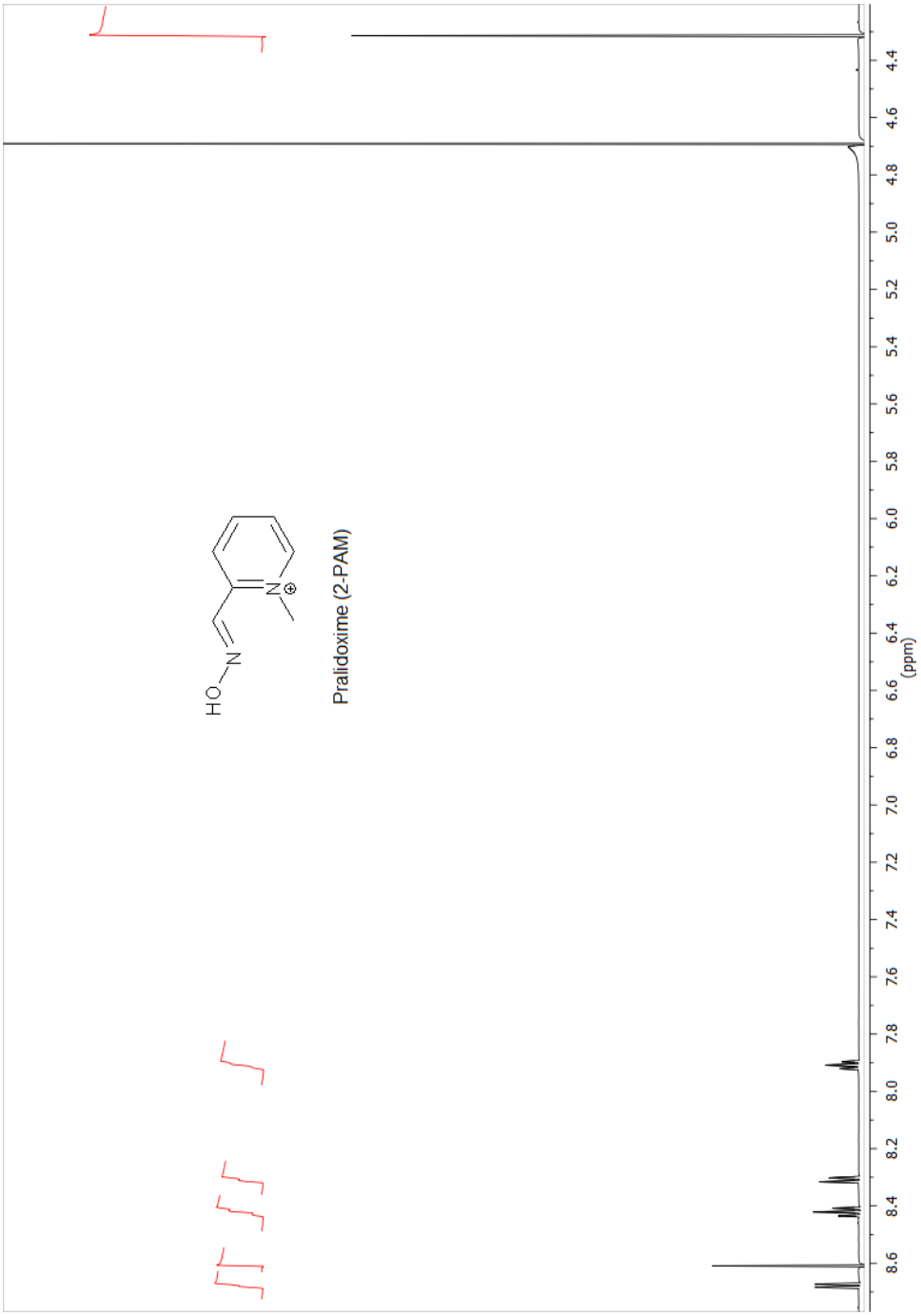

Figure III.3: ^{1}H NMR (600 MHz) spectrum of pralidoxime in deuterated phosphate buffer, pD 6.4. Peak integrals are located above their respective peaks. The peak at δ_H = 4.7 ppm is H_2O

Table III.1: ^{1}H NMR data of pralidoxime in deuterated phosphate buffer, pD 6.4

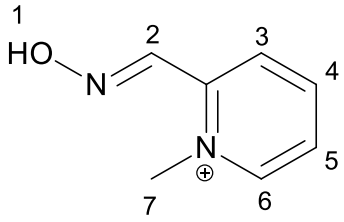

Position	Type	δ_H (ppm)
1	OH	-
2	CH	8.57
3	CH	8.31
4	CH	8.39
5	CH	7.86
6	CH	8.64
7	CH_3	4.29

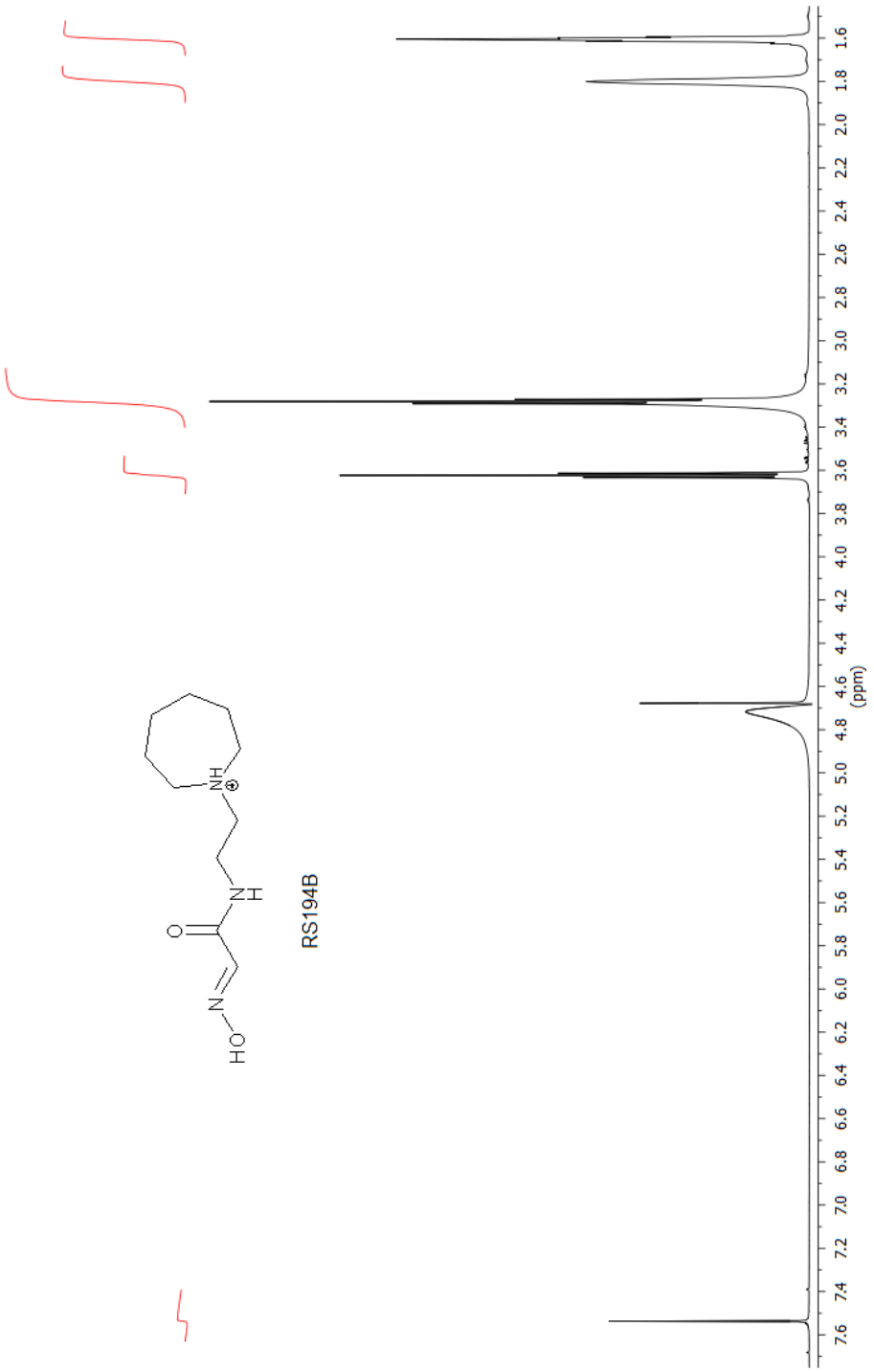

Figure III.4: ^{1}H NMR (600 MHz) spectrum of RS194B in deuterated phosphate buffer, pD 6.4
Peak integrals are located above their respective peaks. The peak at δ_H = 4.7 ppm is H_2O

Table III.2: ^{1}H NMR data of RS194B in deuterated phosphate buffer, pD 6.4

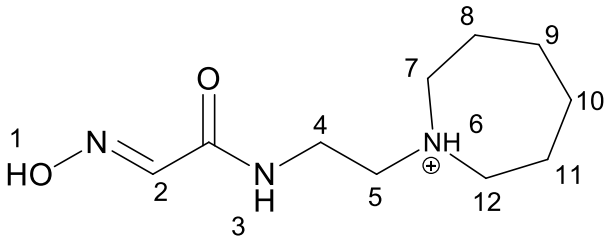

Position	Type	δ_H (ppm)
1	OH	-
2	CH	7.65
3	NH	-
4	CH_2	3.65
5	CH_2	3.30
6	NH	-
7	CH_3	3.30
8	CH_2	1.80
9	CH_2	1.47
10	CH_2	1.47
11	CH_2	1.80
12	CH_2	3.30

D. Kinetic Isotope Studies of on Oximolysis

Kinetic isotope studies on oximolysis were performed by reacting deuterated variants of pralidoxime (D-2-PAM) and RS194B (D-RS194B) with acetylthiocholine in deuterated buffers ranging from pD 5-12. The pseudo-first order rate constants for D-2-PAM and D-RS194B induced oximolysis at varying pD values are summarized in Figure III.5 and are superimposed over their respective nondeuterated pH-dependent oximolysis of ATCh. Both deuterated oximes demonstrated similar sigmoidal pH dependencies with their respective non-deuterated oximolysis experiments, with the difference being a rightward shift in the points of inflection. The points of inflection for the pH-dependence of oximolysis of ATCh are around pH 8.1 for 2-PAM, pD 8.7 for D-2-PAM pH 9.0 for RS194B, and pD 9.8 for D-RS194B. There are no significant changes in maximal nucleophilicity in the deuterated oximes compared to their nondeuterated counterparts.

E. Kinetic Isotope Studies on Oxime-Induced Reactivation of Organophosphate-Conjugated Acetylcholinesterase

VX-conjugated hAChE-WT was incubated at 37 ℃ with deuterated pralidoxime and RS194B in deuterated buffer, ranging from pD 6-9.5. The pseudo first-order rate constants for deuterated 2-PAM and RS194B-induced reactivation of OP-hAChE at various pD values are summarized in Figure III.6 and are superimposed over their respective nondeuterated oxime reactivation experiments from Figure III.3. Both oximes demonstrated a similar bell-shaped pH dependence as their nondeuterated counterparts. Peak reactivation rates occurred at between pD 7.8-8.2 for both deuterated oximes at concentrations above and below their respective K_{OX}. D-2-PAM demonstrated a drop in

maximal reactivation rates by approximately 50% compared to nondeuterated 2-PAM for both oxime concentrations. 5 mM D-RS194B demonstrated a drop in maximal reactivation rates by approximately 30% compared to nondeuterated RS194B and no significant change in maximum reactivation rate for 0.5 mM D-RS194B.

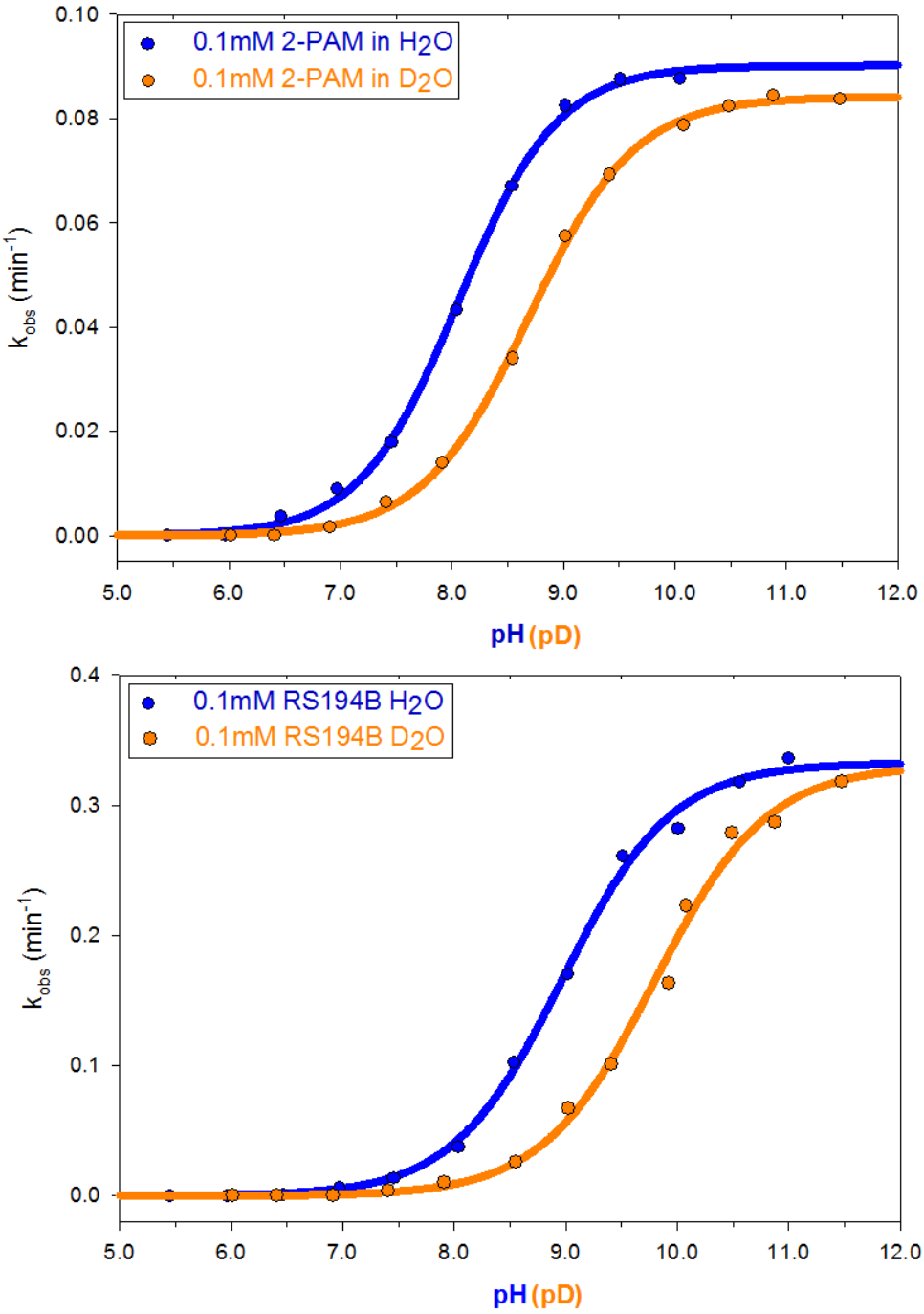

Figure III.5: pH-dependent kinetic isotope studies of 2-PAM and RS194B-induced oximolysis of acetylthiocholine. The upper graph shows pH dependence of 2-PAM-induced oximolysis, while the lower graph shows pH dependence of RS194B-induced oximolysis. Experiments performed in D_2O (orange) are superimposed with experiments performed in H_2O (blue). The points of inflection are approximately pH 8.1 for 2-PAM, pD 8.7 for D-2-PAM pH 9.0 for RS194B, and pD 9.8 for D-RS194B

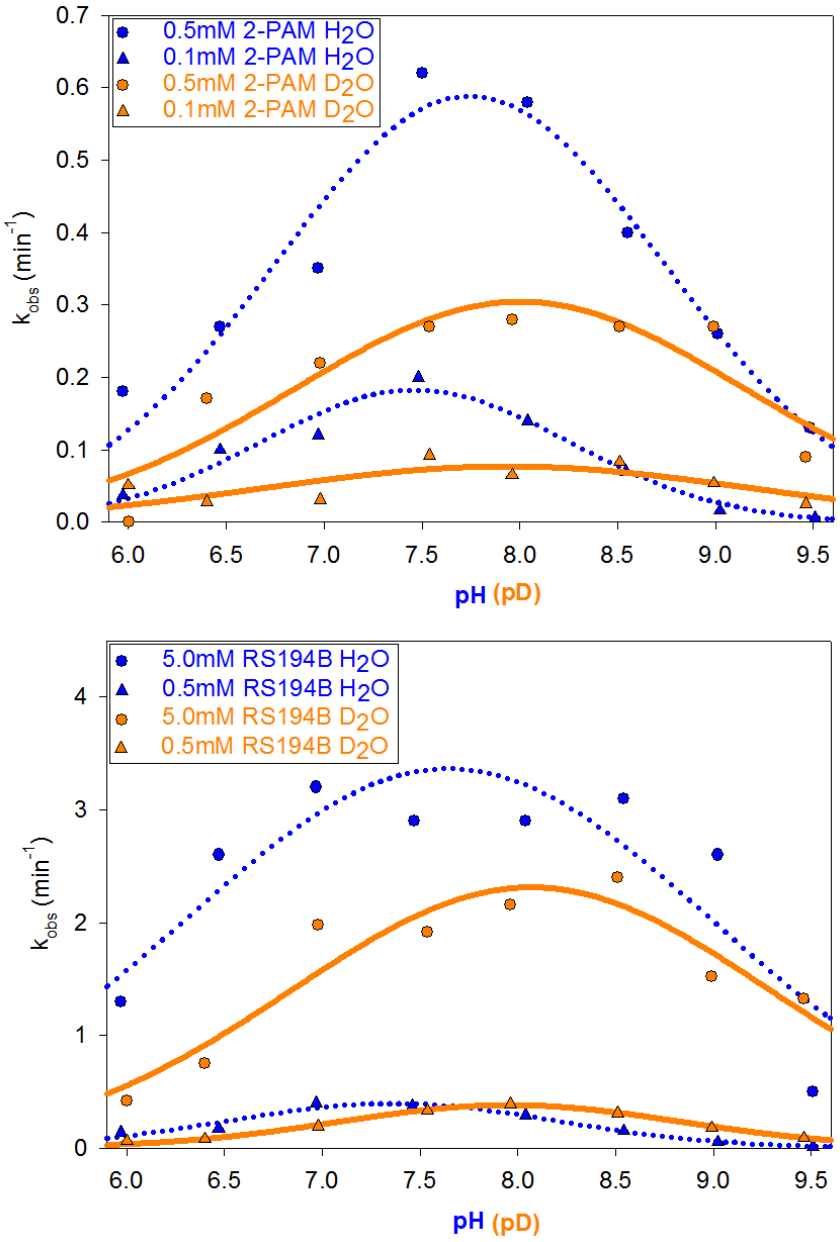

Figure III.6: pH-dependent kinetic isotope studies of 2-PAM and RS194B-induced reactivation of VX-conjugated WT-human acetylcholinesterase. The upper graph shows pH dependence of 2-PAM-induced reactivation rate constants in D_2O. The lower graph shows pH dependence of RS194B-induced reactivation rate constants in D_2O. The deuterium experiments (orange) are superimposed over their respective nondeuterated experiments (blue). Peak reactivation rates occur between pD 7.8-8.2 for both deuterated oximes at concentrations above and below their respective K_{OX}. D-2-PAM shows a greater depression in reactivation rates than D-RS194B

F. pH Dependence of Fluoride-Induced Reactivation of Organophosphate-Conjugated Acetylcholinesterase

Paraoxon-conjugated hAChE-WT was incubated at 37 ℃ with sodium fluoride in buffer solutions ranging from pH 5-9.5. The pseudo-first order rate constants for fluoride-induced reactivation of POX-hAChE at varying pH are summarized in Figure III.7. Reactivation rate constants demonstrated an inverse relationship with pH, with higher rate constants occurred at lower pH values.

G. Kinetic Isotope Studies on Fluoride-Induced Reactivation of Organophosphate-Conjugated Acetylcholinesterase

Paraoxon-conjugated hAChE-WT was incubated at 37 ℃ with NaF in deuterated buffer, ranging from pD 6-8. The pseudo-first order rate constants for fluoride-induced reactivation of POX-hAChE in deuterated buffer for this pH range are summarized in Figure III.8 and superimposed with the data of 10 mM fluoride-induced reactivation in nondeuterated buffer. Data is not fully conclusive, but appears to indicate a rightward shift towards higher pH (pD) values, similar to the results of previous deuterium experiments, but without the depression in reactivation rates.

H. Influence of Ionic Strength on Fluoride-Induced Reactivation

Paraoxon-conjugated hAChE-WT was incubated at 37 ℃ in 10 mM sodium phosphate buffer, pH 6.47, with 10 mM fluoride and chloride concentrations ranging from 0-1 M. The counterions (sodium, lithium, and cesium) were kept consistent between the fluoride and chloride salts. The pseudo-first order rate constants for fluoride-induced reactivation of POX-hAChE with the different cations and different ionic strengths are

summarized in Figure III.9. Reactivation rate constants demonstrated a direct relationship with ionic strength, with increased reactivation rates occurring at higher ionic strengths. Cesium fluoride with cesium chloride also demonstrated higher reactivation rates at ionic strengths ≥ 100 mM compared to NaF with NaCl and LiF with LiCl.

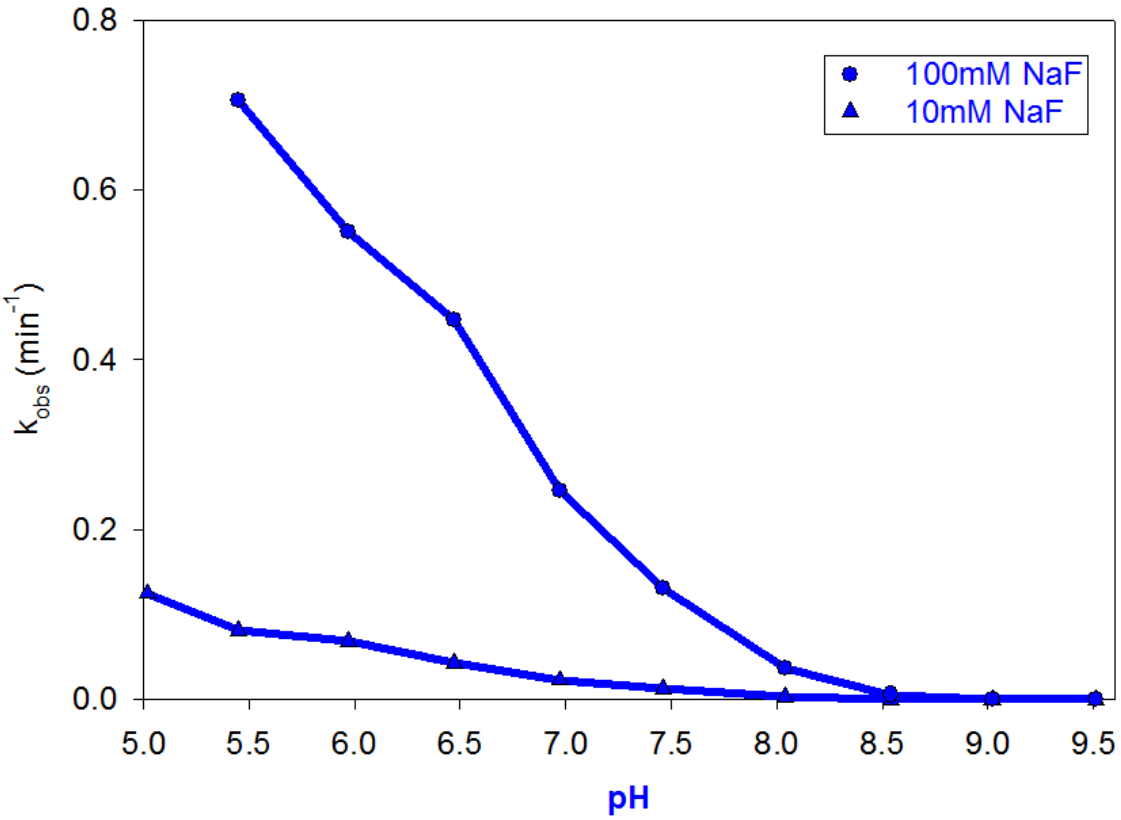

Figure III.7: pH dependence of fluoride-induced reactivation of POX-conjugated WT-hAChE. Reactivation using sodium fluoride demonstrated an inverse relationship between pH and reactivation rate for both 10 mM NaF and 100 mM NaF.

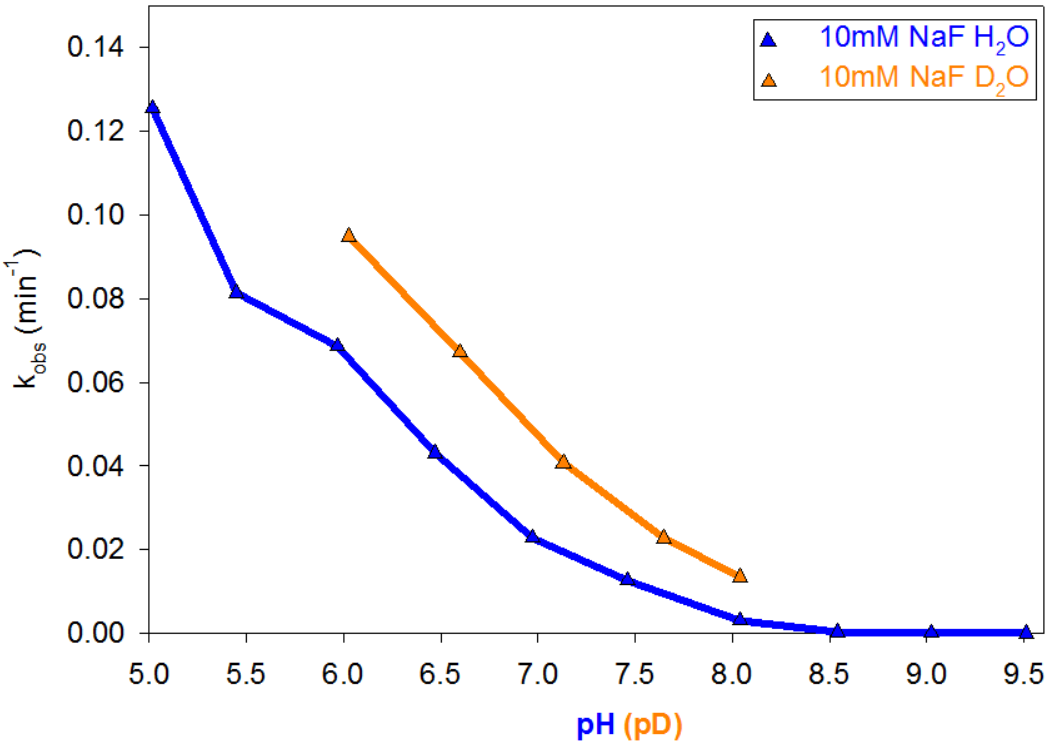

Figure III.8: pH dependence of fluoride-induced reactivation of POX-conjugated WT-hAChE in deuterated buffer. Results for 10 mM fluoride-induced reactivation in D_2O (orange) were superimposed with the data of 10 mM fluoride-induced reactivation in nondeuterated buffer (blue). Data of deuterated fluoride-induced reactivation suggests inverse relationship between pD and reactivation rates, with a rightward shift of the curve compared to nondeuterated fluoride-induced reactivation.

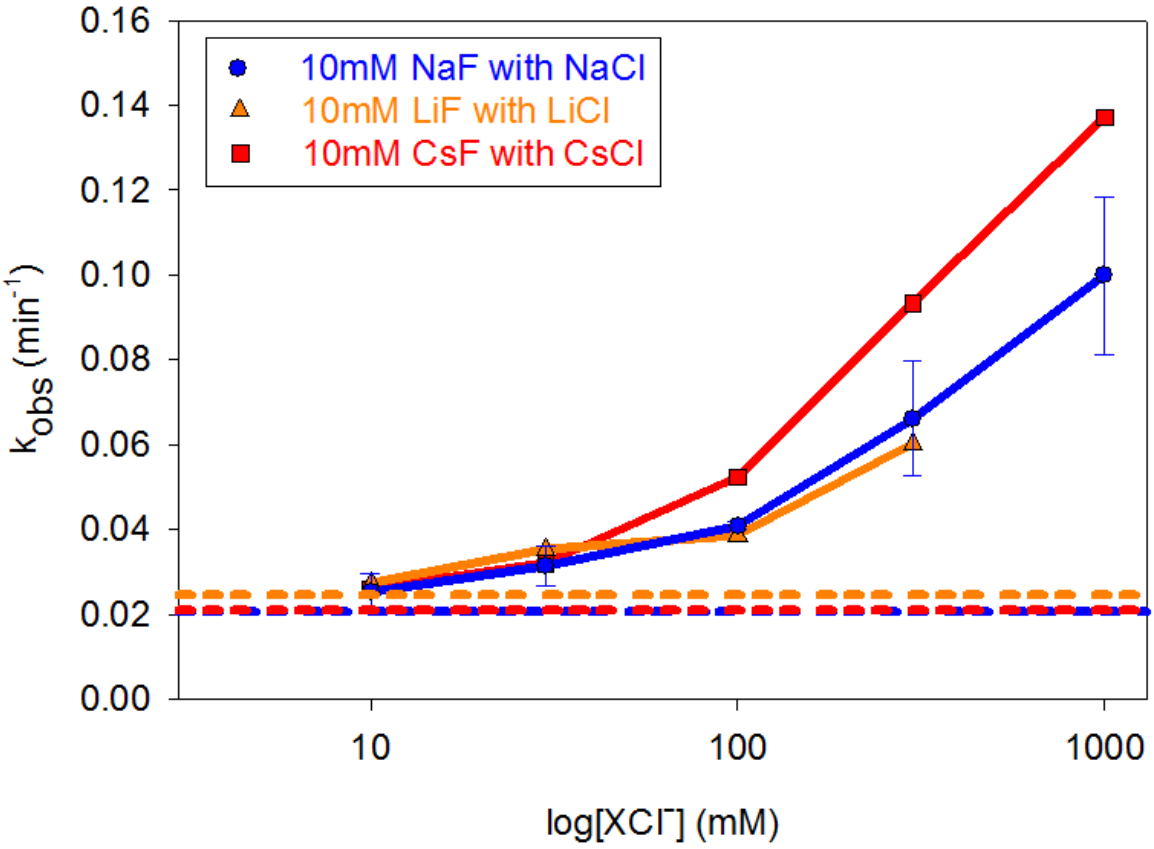

Figure III.9: Ionic strength dependence of fluoride-induced reactivation of POX-conjugated WT-hAChE. Reactivations were performed in 0.01 M sodium phosphate buffer. Ionic strength was controlled using chloride salts, with the counterion being equivalent to the fluoride salt used for reactivation. The dashed asymptotes represent 0 mM chloride concentrations. All three fluoride reactivations demonstrated higher reactivation rates with higher ionic strength. Cesium counterion reactivations demonstrated higher reactivation rates than the lithium and sodium counterion reactivations at chloride concentrations greater than 100 mM.

I. Acknowledgement

This section, in part is currently being prepared for submission for publication of the material with coauthors Zoran Radic, Palmer Taylor, and Limin Zhang. The thesis author was the primary author of this material.

IV.

Discussion

A. Oxime-Induced Reactivation of Organophosphate-Conjugated Acetylcholinesterase

Oxime nucleophilicity shows distinctive behavior for acetylcholinesterase when compared with general base catalysis, as evident by differing pH dependence between in-solution oximolysis and oxime-induced reactivation of OP-AChE. In solution, both 2-PAM and RS194B-induced oximolysis was shown to follow general base catalysis by increasing in rate with respect to pH and substantially increase as the pH approached the oximes' respective pK_a (Radic et al., 2012). Such pH dependence is no surprise, since the oxime is more nucleophilic in its oximate anion species and the pK_a defines the oximate/oxime ratio at different pH values.

However, oxime-induced reactivation of OP-AChE demonstrated no substantial rise in reactivation rate as the pH approached the pK_a for both 2-PAM and RS194B. Rather than the sigmoidal pH dependence shown in oximolysis, oxime-induced reactivation revealed a bell-shaped curve, with optimal reactivation rates occurring at around physiological pH. As a result, reactivation of OP-AChE does not appear to follow general base catalysis, especially considering that both 2-PAM and RS194B exist primarily in their conjugate acid state in this pH range. In addition, there is no significant difference in the optimal pH required for reactivation for 2-PAM and RS194B, despite the fact that their pK_a values differ nearly by a whole pH unit, which further disputes the idea that the oxime simply acts as a general base catalyst in hydrolyzing the phosphoester.

An alternative hypothesis supports the existence of a hydrogen bonding network within the active gorge of the enzyme that is facilitating the deprotonation of the oxime. One proposed network could be the hydrogen bonding between His447 and Glu334 of the catalytic triad. Normally, these two amino acid residues play a role in the charge relay system that deprotonates Ser203 in acetylcholine catalysis, so the idea that these amino acid residues assist in deprotonation of an oxime is tenable. Crystal structures from previous oxime-induced reactivation studies (Figure IV.1) have shown the oxime functional group to be ~3 Å from His447, which is well within the distance to support hydrogen bonding (Kovalevsky et al., 2016).

Furthermore, similar kinetic patterns between oxime-induced reactivation of OP-AChE and normal acetylcholine catalysis supports a role for the catalytic triad participating in oxime-induced reactivation. Acetylcholinesterase catalysis is known to have optimal turnover rates occurring in the range of pH 7.5-8 (Herz and Kaplan, 1973). This optimal pH for catalysis is consistent with the optimal pH for oxime-induced reactivation, which suggests similarity between the two mechanisms.

Previous studies on solvent isotope effects for AChE catalysis of acetylcholine in D_2O have demonstrated a reduced turnover rate by approximately 40% (Malany et al., 2000). This reduced rate was the result of rate limitation on acylation, which is imposed by the transition state of proton (deuteron) exchange between Ser203 and His447 as a part of the catalytic activity. 2-PAM induced reactivation in D_2O demonstrated similar depressions in reactivation rate, which suggests similar rate limitations that are imposed from a possible proton (deuteron) exchange between the oxime and His447.

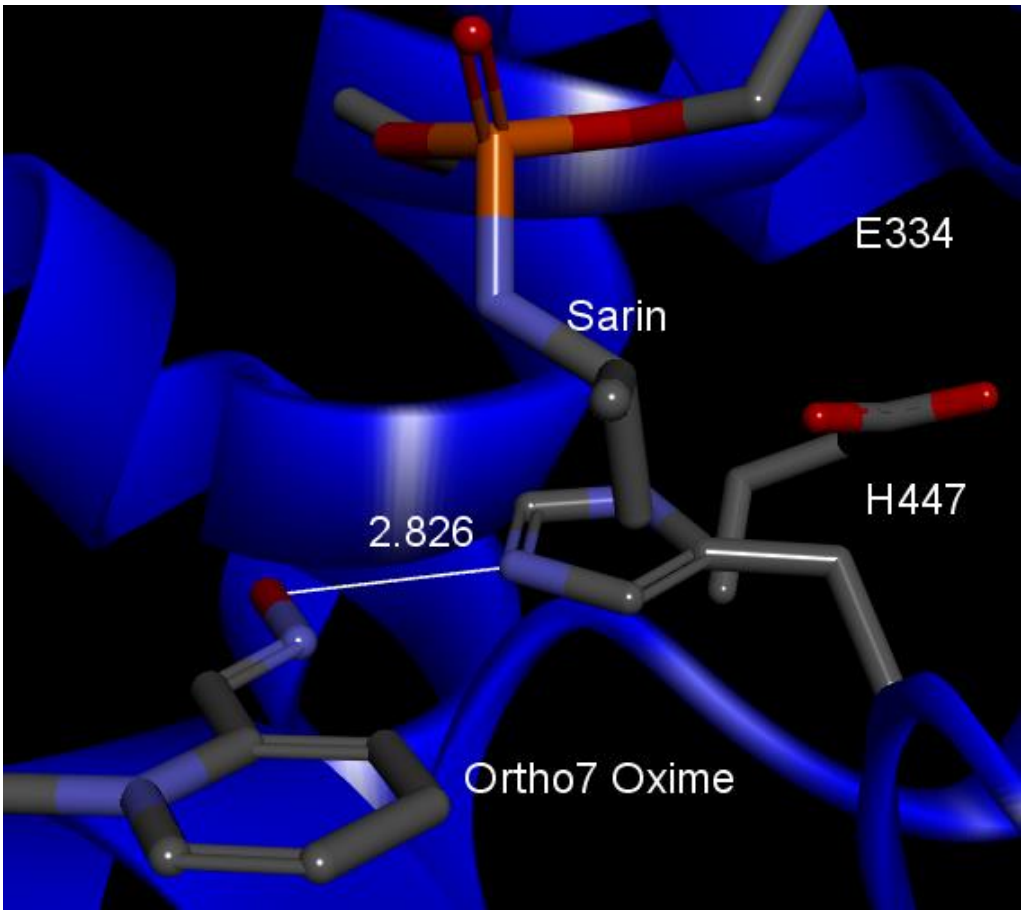

Figure IV.1: X-ray structure of acetylcholinesterase that suggests hydrogen bonding between the oxime and histidine in oxime-induced reactivation (Kovalevsky et al., 2016)

Unlike 2-PAM, RS194B did not demonstrate the same degree of kinetic isotope effect, with only a 30% depression in reactivation rates at oxime concentrations above the K_{OX} value and no significant drop in reactivation rates at oxime concentrations below the K_{OX} value. This lack of kinetic isotope effect could be explained by the hydrogen-deuterium exchange on the tertiary amine on the azepane ring of RS194B that was apparent in RS194B's NMR spectrum. Previous NMR studies on RS194B determined the pK_a of the tertiary amine to increase in D_2O, which would result in higher concentrations of the cationic species (Radic et al., 2012). The higher cationic species would shift the K_{OX} equilibrium towards the oxime*enzyme reversible complex, since the cationic species enters and binds to the gorge more readily, thus reducing K_{OX}. The drop in K_{OX} would compete with the rate retardation (drop in k_2) that is the result of deuterium transfer between the oxime and histidine. D-RS194B concentrations above K_{OX} (less affected by K_{OX}) demonstrated a lesser degree of this competing rate enhancement than concentrations below K_{OX} (more affected by K_{OX}), which is consistent with this theory, and I would expect higher concentrations of D-RS194B, where rate is determined by mostly by k_2, to approach the same rate retardation that is shown in D-2-PAM.

Taking into account of this hydrogen bonding system consisting of His447 and Glu334, I can explain the basis for the bell-shaped curve of oxime-induced reactivation. In general, acetylcholinesterase evolved to function at physiological pH, therefore the enzyme is most stable at physiological pH. If placed in too acidic or too basic pH environments, charged amino acids within the enzyme may gain or lose their charge, which can disrupt the enzyme's conformation. Any structural alignment and dynamics of hydrogen bonding networks that are encompassed by AChE would be disrupted,

therefore exploiting this hydrogen bonding network for oxime deprotonation would also be disrupted at non-physiological pH.

A more in-depth analysis of the formation of this bell-shaped curve is most likely the result of opposing sigmoidal curves (Figure IV.2) that are imposed by different pK_a. The upward sloping curve on the left would induce reactivation at higher pH when the conjugate base species is predominant, therefore I can suggest that this curve represents the pK_a of His447. His447 must be in a conjugate base species in order to induce reactivation, since the protonated conjugate acid species of His447 cannot accept a proton from the oxime. At lower pH, the conjugate acid species would predominate and thus deprotonation is minimalized, which would explain why reactivation rates are reduced at lower pH.

The downward sloping curve on the right would induce reactivation when the conjugate acid species is predominant, therefore I can suggest that this curve represents the pKa of the oxime. The dipole moment of AChE readily accepts cations into the gorge, and the negative charge of the conjugate base species may hinder the molecule's ability to readily enter the gorge. As a result, the oxime cannot enter the gorge to nucleophilic attack the organophosphate, which would explain why reactivation rates are reduced at higher pH.

The overlap of these two sigmoidal curves gives us a bell-shaped curve that contains an optimal "sweet spot" pH for oxime-induced reactivation. However, this example does not take into account for the different pK_a of RS194B and 2-PAM, which is why I emphasize that this example is a very oversimplified version of a complicated model. There are most likely many sigmoidal curves, such as the pK_a of charged amino

acids that contribute to AChE's dipole or oxime binding, as well as the other acidic hydrogen on RS194B, but the idea that their net overlap creates a bell-shaped curve still holds true.

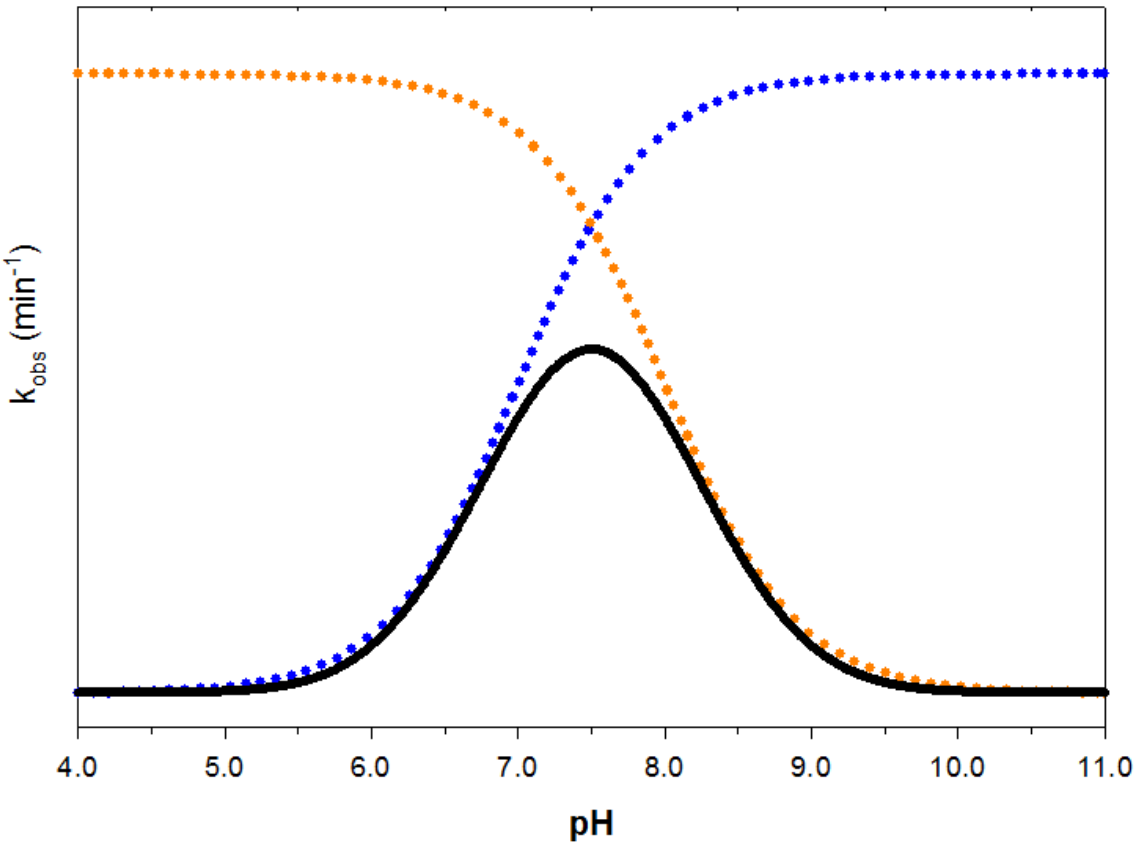

Figure IV.2: Opposing sigmoidal curves model and the resulting bell-shaped curve. The upward sloping curve on the left (blue) represents reactivation that follows the deprotonation of His447. The downward sloping curve on the right (orange) represents reactivation that follows protonation of the oxime.

B. Fluoride-Induced Reactivation of Organophosphate-Conjugated Acetylcholinesterase

Fluoride's ability to reactivate organophosphate-conjugated acetylcholinesterase is very baffling. Acetylcholinesterase contains a dipole moment parallel to the gorge, which directs positively charged molecules, such as acetylcholine into the active site. Amine containing oximes bear a positive charge, which explains how they can readily enter the active gorge and reactivate OP-AChE. On the other hand, fluoride anions are negatively charged and therefore should not readily enter the active gorge, which contradicts the idea that they can reactivate OP-AChE. Since hydrogen fluoride has a pK_a 3.19, there is less than 1% HF concentration in the pH range studied, thus we can rule out any significant impact that the neutral HF may have on reactivation (Vanderborgh, 1968).

Fluoride's small size may explain why it is able to induce reactivation, as its ionic radius (1.33 Å) rivals the Van der Waals radius of water (1.4 Å), which may allow the anion to slip through small side doors that are normally accessible for only water and lead into the gorge as opposed to entering via the same pathway that acetylcholine and oximes take (Shannon et al., 1968; Felix, 2000). Attempts to reactivate with larger anions, such as chloride (1.81 Å) and cyanide (1.92 Å), proved to be fruitless, which supports the theory that fluoride's small size allows it to enter the gorge and attack the organophosphate (Shannon et al., 1968; Morris et al., 1961).

Unlike oximes, which demonstrate optimal reactivation rates at neutral pH values, fluoride-induced reactivation of OP-AChE increases as the pH of the environment drops, making the reaction acid catalyzed. Acid-catalyzed hydrolysis is not unheard of, so the idea of acid-catalyzed fluorolysis may not initially seem farfetched. However, attempts to

induce in-solution fluorolysis of acetylthiocholine at different pH was shown to be fruitless, which is not surprising considering that fluoride ions are weak nucleophiles in aqueous environments due to readily forming hydration shells that impede nucleophilic attack. If we consider fluoride's nucleophilicity to be hindered in aqueous environments, then we must accept that the anion must be stripped of its hydration shell inside the gorge prior to nucleophilic attack of the organophosphate.

An alternative explanation for the pH-dependence of fluoride-induced reactivation is that acidic conditions force the protonation of amino acid residues on the enzyme, and these positively-charged protonated amino acids may allow fluoride to attack the organophosphate. While the kinetic isotope studies of fluoride-induced reactivation of OP-AChE are not fully conclusive and further examination of the extreme pH values is needed, we can interpret that there is a rightward shift in the pH dependence, similar to the kinetic isotope studies in oximolysis and oxime-induced reactivation. However, we have already established that hydrogen fluoride is nearly non-existent in the pH range that was studied, therefore any pK_a shift for hydrogen fluoride is unlikely to be seen. This does not hold true for protonatable amino acid residues, which may assume a pK_a shift from being deuterated, thus backing this idea that protonation of amino acid residues in AChE is contributing to fluoride's reactivation capabilities. Furthermore, there is no sign of depression in reactivation rates in D_2O, which suggests that no sort of hydrogen transfer is occurring for fluoride-induced reactivation as opposed to oxime-induced reactivation.

Interestingly, a study on fluoride reversible inhibition of AChE have demonstrated higher inhibition at lower pH, which may be associated with fluoride's

ability to reactivate OP-AChE due to similar pH dependence and the fact that both scenarios require fluoride to enter the active gorge (Krupka, 1966). The study suggested that interaction between fluoride and a catalytic basic residue (presumably His447) stabilizes the conjugate acid species, therefore blocking catalytic activity. Fluoride binding to a protonated His447 may allow it to position itself for nucleophilic attack on the organophosphate, which may explain why acidic conditions enhance fluoride-induced reactivation because His447 is protonated at lower pH. In addition, Krupka's study showed that cationic inhibitors, like trimethylammonium, bind to the anionic site and interfere with fluoride inhibition, which would suggest further studies on the possibility that trimethylammonium may impede fluoride-induced reactivation.

Another related study on a G117H mutant of human butyrylcholinesterase provided crystal structures of fluoride anions interacting with the imidazole ring of a newly formed His117 mutant (Nachon et al., 2011). Although the crystal structures are of butyrylcholinesterase, a relative of acetylcholinesterase, and that the histidine of interest is not the member of the catalytic triad, the structures suggest that fluoride anions are capable of entering the active site of AChE and interacting with residues within the gorge, which could position the anion for nucleophilic attack against the organophosphate.

As with pH being a factor that affects reactivation rates, ionic strength also appears to contribute to fluoride-induced reactivation of OP-AChE, with higher reactivation rates occurring at higher ionic strength concentrations. What may be believed to be the cause of this phenomena is that the increased ionic strength results in higher concentrations of cationic counterions, which can interact with negatively charged and

aromatic amino acid sidechains located within the gorge. Similar to acidic pH, the presence of cations within the gorge can establish positive charges and reduce negative charges, which could help draw fluoride anions into close proximity of the organophosphate, enabling it for nucleophilic attack.

Another theory is that the higher concentrations of cationic counterions contribute to the disruption of the hydration shell that normally surrounds fluoride anions, thus enhancing its nucleophilicity. From this idea, I thought that smaller cations would be more effective at enhancing fluoride-induced reactivation than larger ones, as they would be able to fit into the enzyme's crevices alongside fluoride. However, this theory was shown to be untrue, since there was no apparent difference in fluoride-induced reactivation between lithium and sodium counterions. The larger counterion cesium contradicts this theory, since it demonstrated higher reactivation rates than sodium and lithium. These enhanced reactivation rates only occurred at CsCl concentrations greater than 100 mM, most likely because of competing effects with the 10 mM sodium contained in the phosphate buffer.

Because lithium and sodium counterions do not appear to differ in enhancing reactivation rate, the size of the counterion does not appear to be a contributing factor. Previous studies on the cation effects of the Hofmeister series had shown that cesium cations more readily disrupt the hydrogen bonding between water and an anionic surface than lithium cations do (Nihonyanagi et al., 2014). Although the study showed no data on sodium, the idea that cesium is more chaotropic than the other two cations may explain why it appears to enhance reactivation rates better than sodium and lithium, since cesium

would more effectively liberate fluoride from a hydration shell, thus allowing the anion to readily attack the organophosphate.

References

Amitai, G., Rellie, A., Yacov, G., Yishay, S., Teitlboim, S., Tveria, L., Limanovich, O., Kushnir, M., Meshulam, H. (2007) *Toxicology* **233**, 187-198 (OP derivatives)

Chunyuan, L., Saxena, A., Smith, M., Garcia, G., Radic, Z., Taylor, P., Bhupendra, D. P. (1999) *Biochemistry*, **38**, 9937-9947

Dvir, H., Silman, I., Harel, M., Rosenberry, T., Sussman, J. (2010) *Chem Biol Interact* **187**, 10-22

Eddleston, M., Szinicz, L., Eyer, P., Buckley, N. (2002) *QJM* **95 (5)**, 275-283

Ellman, G. L., Courtney, K. D., Andres, V. J., Featherstone, R. M. (1961) *Biochemical Pharmacology* **7**, 88-95

Felix, F. (2000) *Water: A Matrix of Life: Edition 2* Royal Society of Chemistry, Cambridge

Goldenzweig, A., Goldsmith, M., Hill, S.E., Gertman, O., Laurino, P., Ashani, Y., Dym, O., Unger, T., Albeck, S., Prilusky, J., Lieberman, R.L., Aharoni, A., Silman, I., Sussman, J.L., Tawfik, D.S., Fleishman, S.J., (2016) *Mol Cel* **63**, 337-346

Heilbronn, E. (1965) *Acta Chem Scand* **19**, 1333-1346

Herz, F., Kaplan, E. (1973) *Pediat Rev* **7**, 204-214

Kingsley, P., Barnard, A. (2017, Apr 6) *New York Times*. Retrieved from http://www.nytimes.com

Kovalevsky, A., Blumenthal, D., Cheng, X., Taylor, P., Radic, Z. (2016) *Ann. N.Y. Acad. Sci.* **1378**, 41-49

Kovarik, Z., Radic, Z., Berman, H., Simeon-Rudolf, V., Reiner, E., Taylor, P. (2003) *Biochem J.* **373**, 33-40

Krupka, R. (1966) *Molecular Pharmacology* **2 (6)**, 558-569

Malany, S., Sawai, M., Sikorski, R. S., Seravalli, J., Quinn, D. M., Radic, Z., Taylor, P., Kronman, C., Velan, B., Shafferman, A. (2000) *J Am Chem Soc* **122**, 2981-2987

Morris, D. F. C. (1961) *Acta Crystal* **14**, 547

Nihonyanagi, S., Yamaguchi, S., Tahara, T. (2014) *J Am Chem Soc* **136**, 6155-6158

Paddock, R., Sang-Hun, C. (2017, Feb 23) *New York Times*. Retrieved from http://www.nytimes.com

Patocka, J., Cabal, J., Kuca, K., Jun, D. (2005) *J Appl Biomed* **3**, 91-99 (OP and oxime review)

Polhuijs, M., Langenberg, J., Benschop, H. (1997) *Toxicol Appl Pharmac* **146**, 156-161

Pope, C., Karanth, S., Liu, J. (2005) *Environmental Toxicology and Pharmacology* **19**, 443-446

Nachon, F., Carletti, E., Wandhammer, M., Nicolet, Y., Schopfer, L.M., Masson, P., Lockridge, O. (2011) *J Biol Chem* **434**, 73-82

Ordentlich, A., Barak, D., Kronman, C., Flashner, Y., Leitner, M., Segall, Y., Ariel, N., Cohen, S., Velan, B., Shafferman, A. (1993) *J Biol Chem* **268 (23)** 17083-17095

Ordentlich, A., Barak, D., Kronman, C., Ariel, N., Segall, Y., Velan, B., Shafferman, A. (1998) *J Biol Chem* **273 (31)**, 19509-19517

Radic, Z., Sit, R., Kovarik, Z., Berend, S., Garcia, E., Zhang, L., Amitai, G., Green, C., Radic, B., Fokin, V., Sharpless, K., Taylor, P. (2012) *J Biol Chem* **287**, 11798-11809

Radic, Z., Sit, R., Garcia, E., Zhang, L., Berend, S., Kovarik, Z., Amitai, G., Fokin, V., Sharpless, K., Taylor, P. (2013) *Chem Bio Interact* **203**, 67-71

Shafferman, A., Kronman, C., Flashner, Y., Leitner, M., Grosfeld, H., Ordentlich, A., Gozes, Y., Cohen, S., Ariel, N., Barak, D., Harel, M., Silman, I., Sussman, J., Velan, B. (1992) *J Biol Chem* **267 (25)** 17640-17648

Shannon, R. D., Prewitt, C. T. (1968) *Acta Crystal* **B25**, 925-946

Sirin, G. S., Zhang, Y. (2014) *J Phys Chem A* **118 (39)**, 9132-9139

Sit, R.K., Radić, Z., Gerardi, V., Zhang, L., Garcia, E., Katalinić, M., Amitai, G., Kovarik, Z., Fokin, V.V., Sharpless, K.B., Taylor, P. (2011) *J Biol Chem* **286**,19422-19430.

Vanderborgh, N. (1968) *Talanta* **15 (10)**, 1009-1013

Wilson, I., Ginsburg, S., (1959) *Biochemical Pharmacology* **1 (3)**, 200-206